MAX-PLANCK-INSTITUT FÜR PLASMAPHYSIK

GARCHING BEI MÜNCHEN

Low-Energy Neutral Particle Analysis at the ASDEX Tokamak

H. Verbeek

Max-Planck-Institut für Plasmaphysik
EURATOM Association, D-8046 Garching

IPP 9/50 September 1984

Die nachstehende Arbeit wurde im Rahmen des Vertrages zwischen dem Max-Planck-Institut für Plasmaphysik und der Europäischen Atomgemeinschaft über die Zusammenarbeit auf dem Gebiete der Plasmaphysik durchgeführt.

IPP 9/50

H. Verbeek

Low-Energy Neutral Particle Analysis on the ASDEX tokamak

(in English)

September 1984

Abstract

A time of flight system for the analysis of low energy neutral hydrogen emitted from ASDEX is described. The neutral flux from ASDEX is chopped in bunches of 1 µs by a slotted cylinder driven by a modified turbo-pump. After a flight path of 2 m the particles are detected by a secondary particle detector. Single particle pulses are collected in a multichannel analyzer in the MCS mode with a time resolution of 1 µs. Differential neutral emission spectra are calculated from the arrival time distributions. A number of results are presented to demonstrate the capabilities of the instrument.

Introduction

The energy analysis of neutral hydrogen atoms emitted by a plasma machine is a well established diagnostic tool in fusion research (1),(2). Quantities such as ion temperatures, neutral gas densities and their effects on the power balance and plasma wall interaction can be inferred from the energy distributions of the neutrals created by charge exchange of the plasma ions with neutral gas in the plasma machine The classical method of neutral particle analysis is stripping of the neutrals in a gas cell followed by electromagnetic analysis of the resulting ions. While very successful, this method lacks sensitivity to low-energy neutrals. Below ~200 eV the stripping cross section becomes too small and the energy and angular broadening become excessive. This method is therefore no longer suitable for energies below ~200 eV.

On the other hand, there is a large flux of neutrals with these low energies to the walls. Owing to the high neutral gas density at the plasma edge the cool plasma ions there are charge exchange neutralized and can leave the plasma. As these low- energy particles significantly contribute to the plasma wall- interaction - i.e. recycling and impurity release - it is interesting to determine their fluxes.

An alternative method of analyzing neutral fluxes is time-of-flight spectroscopy. The flux from the tokamak is mechanically chopped into small bunches and the velocity of the neutrals is determined from their flight time to the detector along a given distance. Quantitative detection of the neutrals can be achieved via the release of secondary particles (electrons and/or negative ions) from a suitable metal surface. Systems based on these principles were developed by several groups (3,4). The one most extensively used is the one at PLT by Voss and Cohen (3). They chopped the particle flux from the PLT tokamak by a slotted disk driven by a magnetically suspended vacuum motor. The time-of-flight spectra are obtained from the time-varying output current of an open multiplier which views the Cu-Be detector plate, where secondary particles are released. Our Low Energy Neutral Analyzer - LENA - is different in many aspects, as will be described below.

Vacuum system

The location of the LENA system at the ASDEX tokamak is shown in Fig. 0: it is mounted at the WNW sector of the torus close to the NW neutral beam injector and a movable mushroom limiter. The beam line is positioned 120 mm below the midplane of the ASDEX torus and nearly perpendicular (19.15^{o} off the normal) to the plasma surface. The chopper is 1.72 m away from the torus, i.e. outside the toroidal field, and the detector-to-chopper distance of 2235 mm defines the flight path length. The whole beam line is differentially pumped by 3 turbopumps with a pumping speed of 360 l/s. Most of the beam line is a 100 mm inner diameter tube, only the piece (50 cm long) close to the ASDEX is 50 mm in diameter. The vacuum at the detector is in the 10^{-8} mb range. Just before the plasma shot starts the pressure rises up to 2×10^{-6} mb for a short time owing to the initial filling gas pulse in the first pumping stage, but stays below 3×10^{-7} mb during the entire discharge. (This pressure was measured $\sim$ 1.2 m away from the torus. The pressure could therefore be higher closer to it.)

The chopper

The chopper is a cylinder 60 mm in diameter which has 9 slits 0.15 mm wide and 10 mm long positioned along equally spaced generating lines. Opposite each chopper slit is a slit 4 mm wide (1.5 mm in the first versions). The wide slit is required so that no particles coming through the chopper slit are cut off during flight through the cylinder.Thin and wide slits thus alternate along the generating surface of the cylinder. This chopper, made from a high tensile strength Al-alloy, is mounted on the rotor of a modified turbopump (Turbovac 360 by Leybold-Heraeus). A cross-section of the chopper system is shown in Fig. 2. The chopper does not obstruct the turbo-blades and thus the pump has its original pumping speed. The turbopump protrudes with the chopper into the centre of the beam line. The stator slit width and its position perpendicular to the beam can be varied. A second stator slit positioned 60^{o} from the beam stabor slit serves for a reference pulse. The pump runs with a speed of 760 + 0.3 Hz and produces a

neutral beam pulse every 146 μs. The pulse length is determined by the stator slit width, 1 μs having been chosen so far.

Before installation the accuracy of the chopper was tested. Two laser beams were passed through the beam stator slit and through the reference slit. The light pulses produced by the spinning chopper were measured with fast photodiodes. It was found that the time jitter between pulses was $\prec 0.4$ μs. This jitter is due to the limited accuracy of the angular position of the slits.

Detector

A schematic cross section of the detector is shown in Fig. 3. The neutral particles entering through the aperture A (30 mm dia) impinge on a Cu or Cu-Be plate which serves as a converter electrode. Negatively charged secondary particles (electrons and possibly also H^- ions) released here are accelerated into the first dynode of an open multiplier (Johnston, type MM1). This multiplier is used as single particle counter. In a calibration experiment described in detail in Ref. 5 the number γ_0^- of negative secondary particles per incident neutral hydrogen or deuterium atom was determined as a function of the incident energy. This curve is shown in Fig. 4. The scattering of the measured points show the reproducibility. It seems that the data for D^0 are slightly above the H^0 data. However, in view of the total error bars this was ignored. Within the errors this curve was quite reproducible. No significant differences between a Cu and a Cu-Be plate were observed. It should be mentioned that the plates were gas covered, which seems to be essential for stable operation (6). Our $\gamma(E)$ curve is consistent with the curve obtained in Ref. 6 and used in Ref. 3. The secondary particles are accelerated by 700 V onto the multiplier. The two extra electrodes 1 and 2 shield the particle trajectories from the grounded vacuum vessel walls and focus all particles released at the converter electrode onto the multiplier entrance. By a suitable choice of the voltages at 1 and 2 it was made sure that the entire current leaving the converter electrode reaches the multiplier entrance, i.e. the collecting efficiency is unity.

The multiplier acts as a single particle detector. The total detection efficiency is therefore

$$\delta(E) = (1 - (\exp - \gamma(E)) \eta(E), \qquad (1)$$

where the first factor is the probability that at least one secondary particle is released from the converter electrode (the validity of Poisson statistics being assumed), and η is the probability that the multiplier produces an output pulse (above a threshold) when a secondary particle impinges. It was attempted to determine $\delta(E)$ direct in the calibration experiment. A weak neutral beam (10^{-12} to 10^{-11} A equivalent) impinged on the converter electrode and the resulting count rate of the multiplier was monitored. This produced a curve $\delta(E)$ versus E with rather large error bars ($\pm$ 40 %). These errors are mainly due to the difficulty of accurately measuring currents in the 10^{-12} A range. It was possible to determine $\eta(E)$ from eq. (1) and the data for $\gamma(E)$ (measured with neutral currents of 10^{-10} to 10^{-9} A equivalent). It turned out that it can be described between 20 eV and 1000 eV by $\eta(E) = 3.4 \times 10^{-4} E + 0.26$, i.e. there is a slight dependence on energy. This indicates that not only are electrons created at the converter surface but also other particles, i.e. H^- ions, and that the relative amount of H^- depends on the energy.

The value of $\eta(E)$ strongly depends on the multiplier voltage and on the discriminator threshold. Both were chosen quite arbitrarily for the above measurements. On the other hand, $\eta(E)$ turned out to be unstable in time. After a vacuum accident (the turbopumps did not run while the system was under vacuum for a weekend) the multiplier voltage had to be considerably increased to achieve a reasonable output. The absolute magnitude of the fluxes presented below is therefore rather uncertain, while the shapes of the curves are considered to be correct because the shape of the $\delta(E)$ curve is primarily determined by the curve of $\gamma(E)$, which turned out to be stable.

To determine η independently, the following procedure could be used (7): The count rate is determined for a continuous flux of particles as a function of the discriminator level. In a log plot this should give a straight line, which can be extrapolated to zero level. The extrapolated

count rate should correspond to 100 % detection efficiency, and for any chosen level the efficiency could be calculated. A glow discharge in ASDEX provides a convenient and continuous source of neutrals for this purpose. Figure 5 shows the glow discharge count rate as a function of the discriminator level for 4 different multiplier voltages. For levels >400 mV all curves are straight lines. However, they do not intersect at zero level and deviate from straight lines at low levels. This indicates that the count rate at zero level does not correspond to 100 % detection efficiency. This is the case when at least one secondary electron is released at the front end of the multiplier by each particle coming from the converter electrode. This should be independent of the multiplier voltage.
Nevertheless the curves of Fig. 5 can be used as a reference when the multiplier is exchanged.
The use of the tokamak for detector calibration during the plasma start-up phase is discussed in the results section.

Data acquisition

The block diagram of the electronic system is shown in Fig. 1. The counts from the multiplier are passed through a fast amplifier-discriminator Ortec 9301/9302 or Chronetics 156 B/151 and counted in a multichannel analyzer (Le Croy3500) in the multiscaling mode. This is capable of count rates of up to 100 MHz. The light of a He-Ne laser at the reference channel is chopped as the neutral beam. It turned out that the heights of the light pulses are different for the cases where a narrow chopper slit passes the stator slit and a broad slit passes. This provided a convenient means of discriminating from the unwanted light pulses due to the broad slits. The light pulses trigger a timer, which in turn triggers the multichannel analyzer.

It also triggers a high-voltage pulser, which makes the detector sensitive a short time after the start pulse. The detector has to be insensitive at the very beginning to prevent overloading of the multiplier due to photoelectrons produced at the converter electrode by the light and X-ray emission of the tokamak.

Two measuring modes can be applied:

1. The timer triggers a scan over 256 channels of the MCA at each start pulse. The dwell time can be as short as 1 μs. In this mode the channel number corresponds to the flight time t in μs. However, as the reference pulse might come slightly before or after the true start, there can be a time offset t_0, which can be determined when the H V pulses at the detector are turned off and the sharp photoelectron peak due to the light emission of the tokamak is visible. This marks the channel corresponding to the true time zero. t_0 can be adjusted by moving the stator slit in the reference channel perpendicularly to the beam.
The number of scans forming one arrival time distribution can be chosen. After the preselected number of scans a new portion of the memory 256 channels long is addressed. A total of 32 arrival time distributions can be acquired during one shot of ASDEX. The time resolution during an ASDEX shot depends on the preselected number of scans. A minimum time resolution of 20 ms is possible with reasonable statistical fluctuations. An example of an arrival time distribution collected during 100 ms is shown in Fig. 6. At channel 145 a new distribution corresponding to the next chopper slit starts. This is added to the first spectrum in the computer. (The pulses between channels 70 and 140 are due to the broad slits and are ignored.)

2. In this mode the dwell time at each channel determines the time resolution during a shot. By gating the MCA for a time interval Δt all particles arriving in this flight time interval (corresponding to a certain energy interval) are counted. Several shots of the same kind are therefore necessary to study the time evolution of the outflux of neutrals in several energy intervals. A time resolution of 1 ms is possible with acceptable statistical fluctuations.

Data analysis

The LENA system views an elliptical area of the plasma surface 48 mm high and 34 mm wide. The nominal plasma radius of ASDEX is 400 mm.From its geometry the plasma can thus be considered as a plane source of neutral emission. The brightness of the source is therefore independent of the distance, i.e. the emission measured at the stator slit represents that of the plasma. This assumption should be true at least near the direction normal to the plasma surface. Of course, no attenuation must be present.

On these assumptions the differential neutral emission function $(d\Gamma/dE\,d\Omega)_0$ at our angular position ϑ_0 can be determined from the arrival time distributions, i.e. the numbers N(t) counted in each channel corresponding to the time t:

$$(d\Gamma/dE\;d\Omega)_0 = N(t)/(\delta(E)\;A_c \times \Delta\Omega\;\Delta E(t) \times \Delta t_m \qquad (2)$$

(numbers of neutrals/(cm^2· eV·s·ster)),

where $\delta(E)$ is the detection efficiency, A_c the area of the chopper slit, $\Delta\Omega$ the solid angle interval, $\Delta E(t)$ the energy interval corresponding to the channel at time t and Δt_m the effective measuring time. In our case the relation between energy E and flight time t is

$$E/M = 2.6078 \times 10^{-4} \times (t-t_0)^{-2} \quad (eV/M) \qquad (3)$$

where M is the mass number of the neutrals, t is measured in μs, A_c = 0.013 cm^2, $\Delta\Omega = 1{,}72 \times 10^{-4}$ ster, and Δt_m is the opening time of the slit (0.97×10^{-6} s) times the number of scans for the spectrum. Equation (2) holds for the first measuring mode.

For the second measuring mode, where the flux of particles within a certain flight time interval is measured, ΔE corresponds to this time interval.

To evaluate the number of particles emitted per cm^2 of plasma surface, eV, and second, the angular distribution has to be known. In Ref. 3 a cosine distribution was assumed. However, there are probably large deviations from the isotropic emission:

1. It has been observed that the emission is anisotropic at higher energies, giving larger emission at larger angles (8).
2. The generation of neutrals is a volume effect and the neutrals originate from a plasma layer of finite thickness, which depends on the energy of the observed particles. Increased emission at oblique angles therefore can be expected.

To determine these effects observations at different angles to the plasma surface would be necesary. If nevertheless a cosine angular distribution is assumed, it is

$$d\Gamma/dE = (\pi/\cos\vartheta_o)\ (d\Gamma/dE\ d\Omega)_0 \qquad (4)$$

For the plane source assumption, this is also the flux arriving at the wall of the plasma vessel.

From $d\Gamma$ the power flux distribution can also be obtained:

$$dP/dEd\Omega = eE(d\Gamma/dE\ d\Omega) \qquad (5)$$

$$(watt/(cm^2 \cdot eV \cdot ster)).$$

These quantities can be calculated from the data stored on a floppy disk shortly after the experiment.

There are several sources of errors which enter the determination of $d\Gamma/dEd\Omega$: The largest uncertainty in the $d\Gamma/dEd\Omega$ scale (i.e. the height of the curves) is due to the uncertainty of the detection efficiency η as discussed above; it can be a factor of as much as two. The errors of $\gamma(E)$ are largest at the lowest energies and may therefore influence the shape of the spectra.

The timing errors are mainly due to the jitter of the start pulses, which is $<0.4\ \mu s$. This is in addition to the finite open time of $1\ \mu s$. The timing errors influence the shape and via $\Delta E(t)$ also the height of the spectra. They are largest at low channel numbers or high energies. No reasonable data for energies above ~ 2000 eV/amu can therefore be obtained. The lowest detectable energy is given by the $\gamma(E)$ curve, which exists down to 10 eV for Hydrogen, i.e. 20 eV for Deuterium (s. Fig. 4). In many cases, however, no reasonable data can be obtained at these low energies, because of poor counting statistics at the corresponding long flight times (s. Fig. 6).

Results

In this section a few results for different ASDEX shots are presented to demonstrate the capabilities of the LENA system. Some results are quite puzzling and they demonstrate that for an understanding more measurements at different poloidal and toroidal positions and at more angles would be necessary.

The plots of $d\Gamma/dEd\Omega$ shown in the following are taken from hard copies of computer plots on a video display. This causes the step structure seen on most curves.

1. Plasma Start-up Phase:

LENA spectra were recorded during the start- up phase of a series of divertor discharges in deuterium. The plasma current and the line averaged electron density $\bar{n}_e$ at the beginning of these shots are shown in Fig. 7. The linear rise of $\bar{n}_e$ is due to the feedback programmed gas inlet.
The differential flux emission spectra at 0.07 and 0.19 s from the plasma start are shown as examples in Fig. 8. These spectra are averaged over 20 ms. Both spectra are curved in the log plots. This means that at least 2 temperatures can be determined, these being indicated by the straight lines in Fig. 7. The corresponding particles originate from different plasma radii at different temperatures. It is seen that both temperatures increase during plasma build-up. Generally, at later times the slope of the spectra decreases and they are curved lines. This indicates that deeper layers of the plasma as their temperatures increase contribute to the neutral emission.
According to Voss and Cohen (3) the neutral emission during the plasma start-up phase can be correlated to the rate-of-change of the electron density. In the start-up phase the neutral gas serves both as a source of plasma and neutrals by charge exchange from the plasma ions. With some simplifying assumptions the total neutral emission is

$$\Gamma = \frac{3\,V\,\langle \sigma_{cx} \cdot v_i \rangle_{T_i}}{4\,A\,\langle \sigma_{ion} \cdot v_e \rangle_{e}} \cdot \frac{d\bar{n}_e}{dt} \qquad (6)$$

where V and A are the volume and surface area of the plasma, $\langle \sigma_{cx} \cdot v_i \rangle_{T_i}$ is the Maxwellian averaged charge exchange rate coefficient for the ion temperature T at time i, $\langle \sigma_{ion} \cdot v_e \rangle_o$ is the rate coefficient for ionization by electron impact, and $d\bar{n}_e/dt$ is the rate of change of the line averaged electron density. The rate coefficients can be obtained from Ref. 9, V/A is taken as a/2 = 20 cm (a = minor radius), and $d\bar{n}_e/dt$ is determined from Fig.7. The CX-rate coefficient is determined at the lower temperature obtained from the spectra of Fig. 8, since this holds for the majority of the particles.

The result is shown in Fig. 9 (upper curve). For the experimental data the spectra of Fig. 8 have to be integrated over all energies and the solid angle. As the angular distribution is not known, a cosine-distribution was assumed. For a series of shots both the calculated and the experimental results are quite reproducible. For shot #13301 the multiplier voltage was 4 keV, while it was 3.7 keV at shot #13304, yielding a somewhat lower detection efficiency. At the beginning of the discharge the agreement of the two curves for #13301 is within a factor of two, which is quite good in view of the simplifying assumptions. In Ref. 3 the agreement is excellent, and the authors use the calculated Γ to determine the detector efficiency. However, this does not seem to be justified because of the many assumptions.

2. Neutral Injection

In Fig. 10 an ASDEX shot with neutral beam injection is shown. Between 1.1 and 1.3 s a 3.2 MW beam of neutral hydrogen was injected into a deuterium discharge. The rise of $\bar{n}_e$ and the occurrence of bursts in the H_α emission indicate that the shot went into the H-phase (10). The neutral flux spectra averaged over 100 ms during the times indicated in the upper figure are shown in the lower part. Spectrum 1 is typical of ohmic discharges. With neutral injection the intensity first decreases at low energies and increases at energies $>$700 eV (spectrum 2). Then the intensity decreases drastically by 2 orders of magnitude at 500 eV (spectrum 3) and goes up again after the NI is finished (spectrum 4).

This behaviour was not observed with the charge exchange neutral-particle diagnostics positioned at different locations at ASDEX. It cannot readily be explained, but it is quite reproducible. In Fig. 11 the same effect is observed with better time resolution. It also occurred in L-discharges, as is shown in Fig. 12, which was a hydrogen discharge. In this case (# 11061) the decrease is somewhat less compared with #12115 shown in Fig. 9.

In the second measuring mode (see section on data acquisition), where the intensity of neutrals in a certain energy interval is monitored, better time resolution during a shot is possible. In Fig. 13 a series of shots with neutral injection is shown. The neutral flux emission Γ is shown together with $\bar{n}_e$. The H-regime was again reached in all cases. It is seen that at the onset of neutral injection Γ first increases for energies >127 eV and then decreases drastically for energies <800 eV (the two lower curves). The time resolution was 10 ms in these cases.

There are, however, also cases where the drastic decrease during NI does not occur. Examples are shown in Figs. 14 and 15. For Fig. 14 D^0 was injected into a deuterium plasma. After ignition 4 of 8 sources failed, but the H-regime was reached. The differential neutral emission spectra are shown for the two times indicated in the upper figure. $d\Gamma/dEd\Omega$ slightly decreases at energies <300 eV but increases above 300 eV. There is no such large decrease as in Figs. 10 - 12.

This is not seen either in Fig. 15, where measurements with method 2 (constant energy windows) are shown for 3 shots of the same kind. The time resolution here was 1 ms. As seen in the bottom figure $\bar{n}_e$ and FDKU (which is an H_α-signal) show that the H-regime is reached. With the onset of NI the neutral emission increases within about 10 ms in all energy intervals. This increase is largest for the highest energies. After this peak the neutral emission decreases to reach a plateau after about 70 ms. The neutral emission during this time (during the H-phase) is $\sim$10 x as large as during the ohmic phase (# 12682), slightly lower for $127 < E < 880$ eV (shot #12727) and $\sim$10 x as low for $22 < E < 127$ eV (shot #12725). The difference to Fig. 12 is striking. (Note that in Fig. 15 the scale is linear, while it is logarithmic in Fig. 13, shots #10809 and #10810.)

The bursts seen in the H_α-signal should also be visible in the neutral emission when the time resolution is 1 ms. However, only an increase in the scattering of the data points shows up (see Fig. 15, shot #12727). This is due to the fact that these data points are only taken during the short open time (1 μs) of the chopper, which occurs every 146 μs.

The observed behaviour during NI is hard to understand. The sharp decrease in the neutral emission with a minimum at around 500 eV was observed for H- and L-discharges, for H^0 and D^0-injection, and H_2 and D_2- discharges. The only parameter which was different in Figs. 14 and 15 (no decrease) is that the plasma was shifted upward by 2 cm (Z = 2). It is not understood why this causes these large differences in the neutral emission.

It should be mentioned that the plasma region, where the neutral beam of the nearby Nort-West injector is deposited, is out of the line-of-sight of the LENA.
More measurements at different locations at ASDEX would be necessary to find out whether this effect observed at the present location is characteristic of the whole tokamak or only of that particular location. The latter is more probable since the effect was not observed with other neutral particle diagnostics.

3. Lower Hybrid Resonance Heating

In Fig. 16 an ASDEX shot (#11064) is shown with a HF pulse of lower hybrid frequency (1.3 GHz) at a power level of 560 kW during 0.9 to 1.1 s. Two spectra before and during the LH pulse are shown at the bottom. The neutral emission increases during the LH pulse at energies $>$ 200 eV while no change below 200 eV is seen. The same behaviour is seen in Fig. 17, where measurements with a constant energy interval are depicted. The upper right plot shows the sudden increase of the neutral emission with energies $>$ 1000 eV during the LH pulse and the return to the value before at the end of the LH-pulse. (See for comparison the plot without LH at the upper left.) In the lower plots a much smaller increase during LH is observed for $141 < E < 1180$ eV and no change is seen for $E < 141$ eV. The slope of the

tails of the spectra in Fig. 16 decreases during LH. This indicates a rise in temperature of the edge plasma where the observed neutral flux originates. In Fig. 18 the power flux distribution calculated from the same spectra as in Fig. 16 is shown. If complete poloidal and toroidal symmetry is assumed from these spectra the total power loss of the tokamak due to the neutrals can be estimated. Integration yields 0.061 Watt/cm^2 for the additional power loss during LH-heating. For a total plasma surface of 2 x 10^5 cm^2 this amounts to 12 kW i.e. 2 % of the LH heating power.

In Fig. 19 shot #11575 is shown.It was attempted to drive the plasma current by LH-injection (600 kW). The neutral emission spectra show little difference in the ohmic phase (8) and during the LH pulse (10, 16).

4. Limiter Discharges

In Figs. 20 and 21 measurements during a limiter discharge (shot #12090) are shown. With this shot it was intended to produce a plasma with small minor radius. Therefore, the plasma current and $\bar{n}_e$ (shown in Fig. 20) were reduced at 0.5 s, the plasma was moved outward by 9 cm during 0.7 to 0.9 s, the multipole current (MPI) was tuned to zero and the limiter became active. A mushroom limiter was used, which was positioned 5 cm beyond the normal plasma edge and located in the same sector as the LENA. This procedure should reduce the plasma minor radius to 26 cm.

The development of $d\Gamma/dEd\Omega$ averaged over 100 ms is shown in Fig. 21. The intensity over the whole energy range is 5 to 10 x as large as in the divertor discharges shown in Figs. 8 to 19. The good counting statistics allowed to determine $d\Gamma/dEd\Omega$ down to 16 eV for Deuterium. It is remarkable that all spectra still increase at low energies. There is no maximum visible at low energies.

It is seen in Fig. 21 that beginning at 0.3 s up to 0.6 s the spectra show a minimum at ~200 eV. At 0.55 s the intensity at 200 eV is an order of magnitude lower than at the beginning and after 0.7 s when the minimum disappears again. The reduction of the low energy flux occurs when the plasma is shifted outward towards the limiter. That means that the edge

plasma is scraped off, from where the low energy neutrals originate. At later times during the plateau phase of IPLAS and $\bar{n}_e$ (Fig. 20) the edge plasma is re-established and the neutral spectra have their normal shape again.

Conclusions

From the examples discussed in the results section it can be concluded that the Low Energy Neutral Analyzer based on time of flight techniques yields valuable information especially at low energies. In all cases observed so far the number of neutral particles at energies <100 eV emitted from ASDEX increases more than linearly on the log scale with decreasing energy. These particles significantly contribute to the recycling at the wall and - in spite of the low sputtering yields - also to the impurity production (11). The shape of the measured differential neutral emission spectra is considered to be correct within the errors discussed above. The absolute height of the curves, however, still has a larger uncertainty due to our poor knowledge of the detection efficiency. The uncertainty in the detection efficiency can be estimated at a factor of 2 from consideration of the data in Figs. 5 and 9.

The lowest detectable energy is mainly limited by the counting statistics at long flight times. In the case of Fig. 21 data for 16 eV Deuterium could be evaluated. However, in most cases no more valuable data could be derived for energies ≤ 15 eV of Hydrogen, i.e. ≤ 30 eV of Deuterium. The spectra can be evaluated up to ~ 1000 eV for H and 2000 eV for D. Beyond this energy the energy interval corresponding to the channel width of 1 μs is larger than the energy and the errors become excessive.

The time resolution possible during an ASDEX shot is limited by statistics to 20 ms when a whole energy distribution is measured. Thirty spectra of this kind, i.e. a portion of 600 ms of the entire shot, can be observed. Better time resolution of up to 1 ms can be obtained when only a certain energy interval of the whole distribution is monitored. It should be borne in mind, however, that owing to the chopping only 1/146 of the real time is measuring time.

A number of features hard to understand were observed. For an explanation of these data more measurements at different angles and different poloidal and toroidal locations would be necessary. The measurement of the angular distribution of the neutral emission by a LENA system which can view the plasma at different angles would be necessary to determine the neutral flux to the wall. So far, a cosine distribution has had to be assumed for the angular integration, which in all probability is not true.

Acknowledgement

I am indebted to Dr. Götz of Leybold-Heraeus for the realization of the chopper and to Dr. Moritz of LeCroy Research Systems for an ingenious modification of the multichannel analyzer.Thanks are due to W. Eckstein for numerous discussions, to W. Englert for programming the computer, to Mrs. C. Fritsch for measuring and evaluation of the data, and to R. Hippele and S. Schrapel for their technical help.
The collaboration with the ASDEX team is greatly acknowledged.

References

1) M.P. Petrov, Sov.J.Plasma Phys. 2 (1976) 201
2) F. Wagner, J.Vac.Sci.Technol. 20 (1982) 1211
3) D.E. Voss, S.A. Cohen, J.Nucl.Mat. 93/94 (1980) 405
and Report PPPL-1884 (1982)
4) H.J.B.M. Brocken, Rijnhuizen-Report 81-136 (Oct. 1981)
5) H. Verbeek, W. Eckstein, Report IPP 9/45 (1983) and
Verhandl. DPG (VI) 17 (1982) 913
6) J.A. Ray, C.F. Barnett, B. van Zyl, J.Appl.Phys. 50 (1979) 6516
7) R. Izvostshikov, private communication
8) F. Wagner, Proc. NATO Summer School, Val Morin, Canada 1984
9) R.L. Freeman, E.M. Jones, Report CLM-R 137, Culham 1974
10) F. Wagner et al. in Plasma Physics and Controlled Nuclear Fusion
Research 1982, Vol. 1, p. 43; IAEA, Vienna (1983).
11) G. Staudenmaier, Proc. AVS-Symp., Reno, 1984
J.Vac.Sci.Techn., to be published.

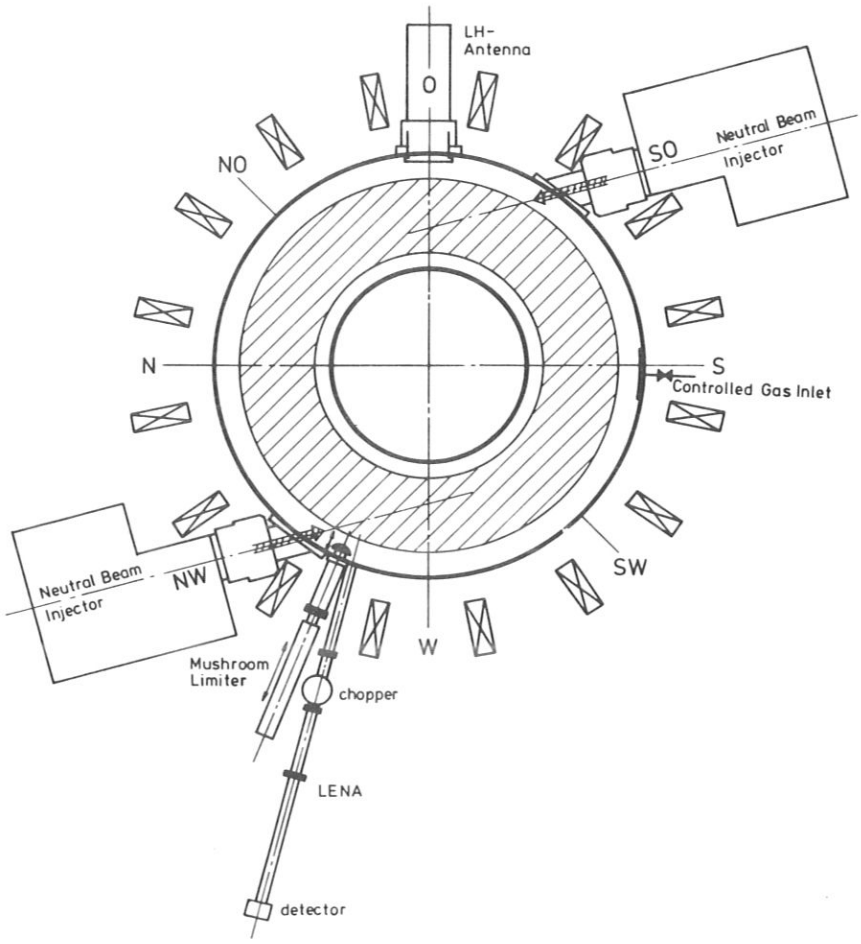

Fig. 0:

Ground plan and cross section of ASDEX with the location of the LENA system

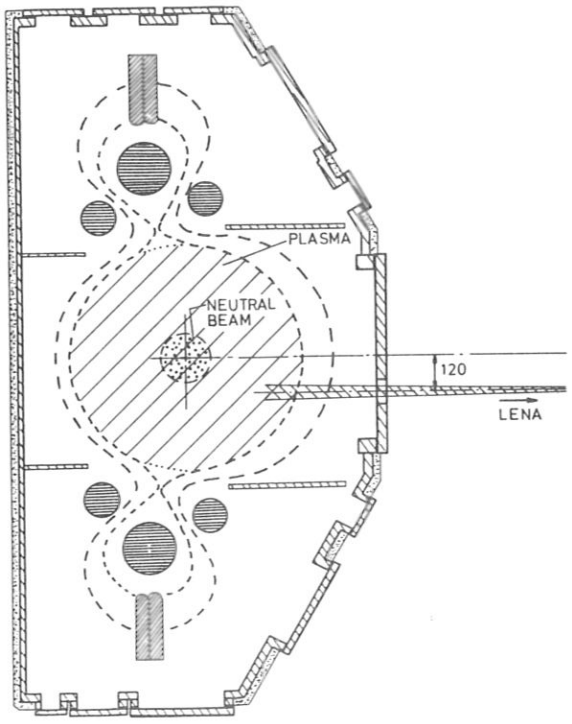

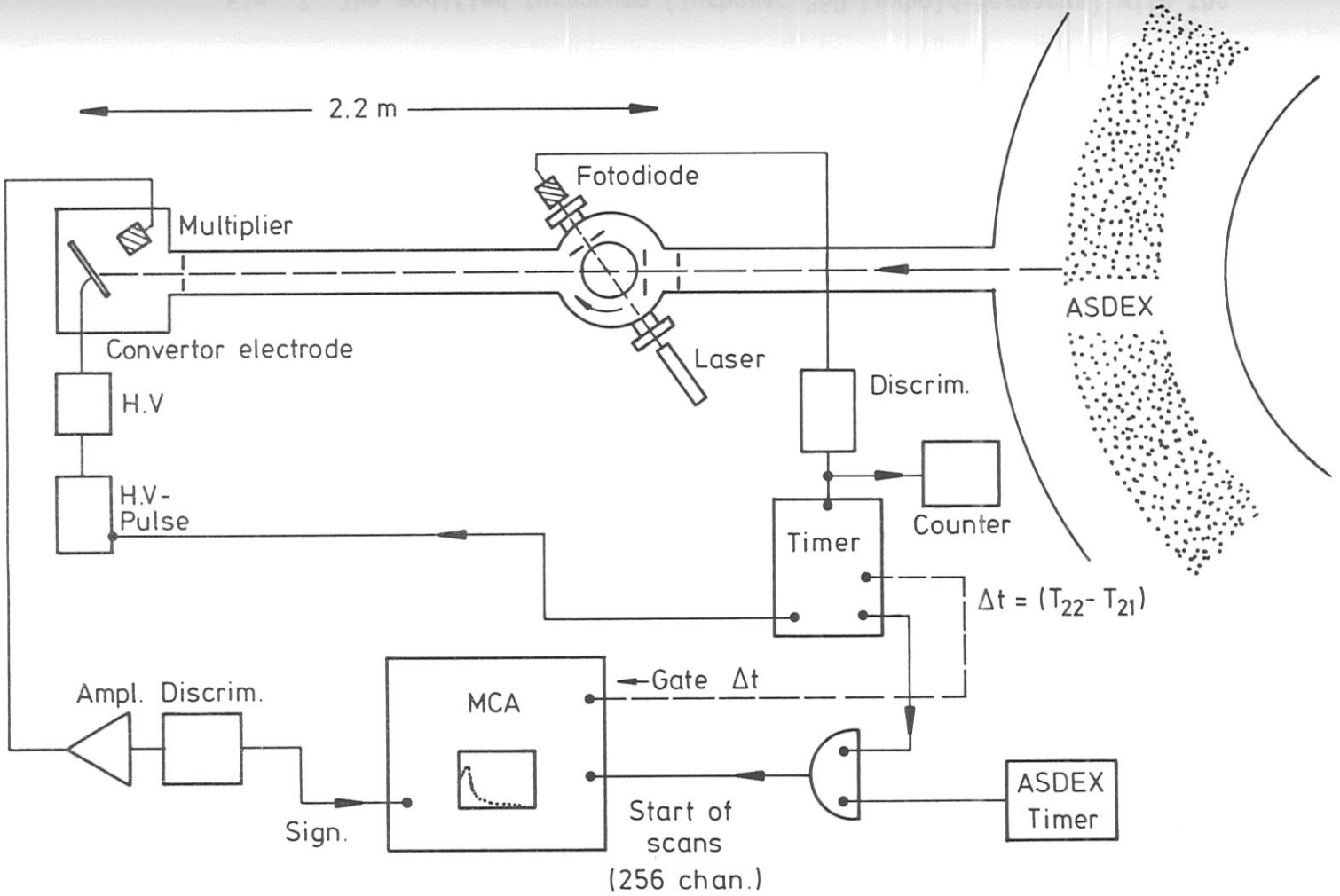

Fig. 1 Schematic of the time-of-flight system with the electronics

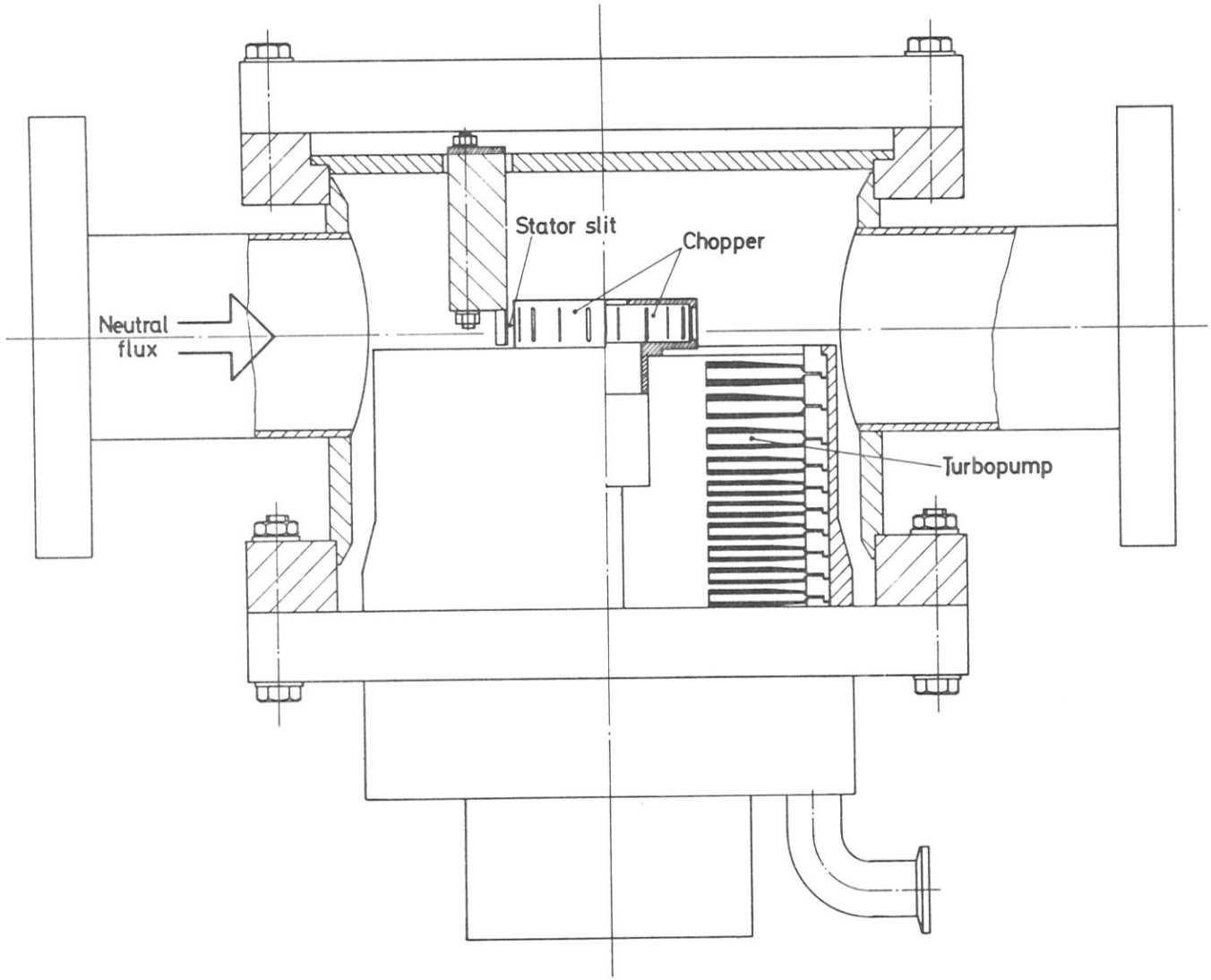

Fig. 2 The modified turbopump (Turbovac 360 Leybold-Hereaeus) with the beam chopper

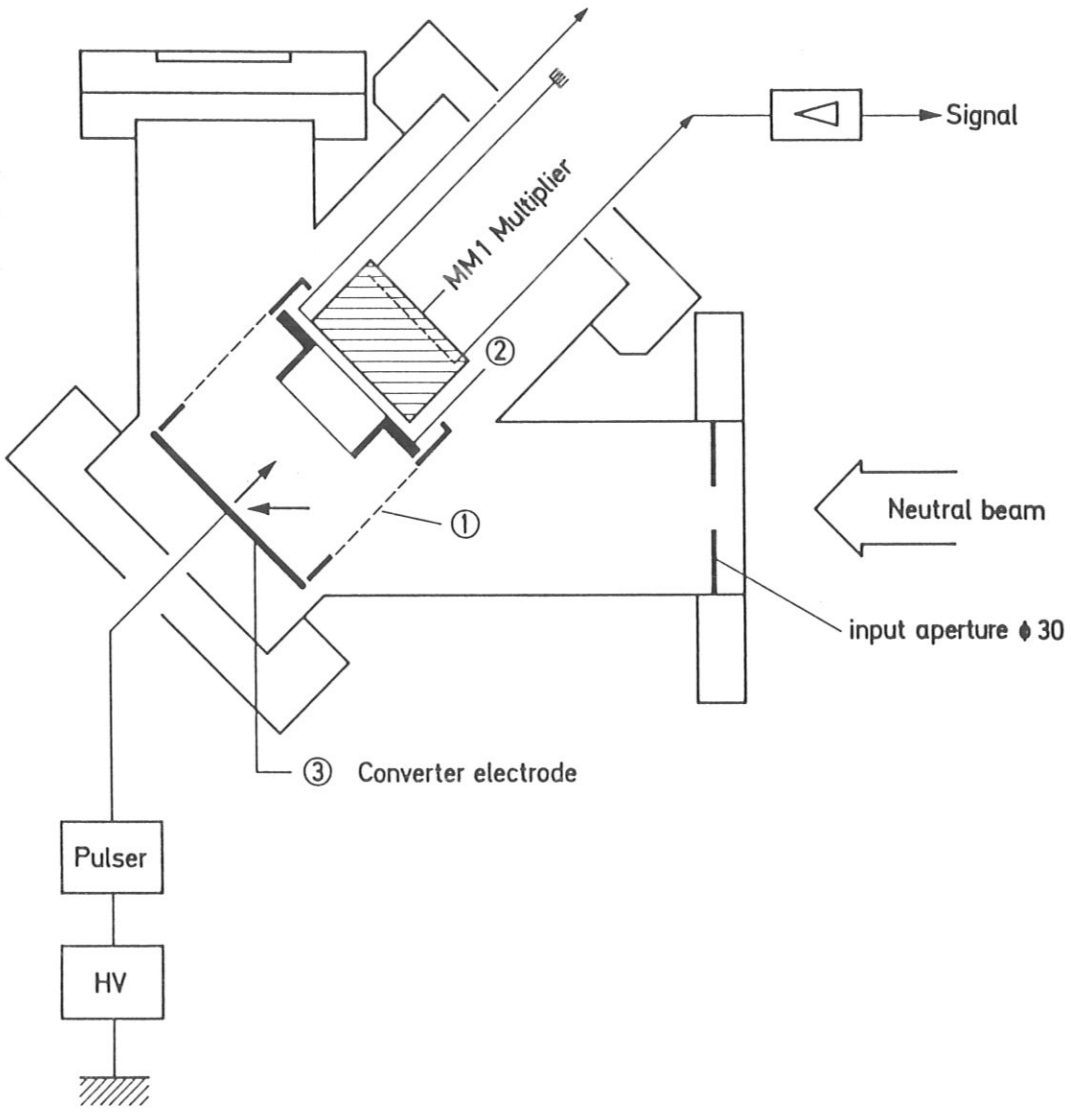

Fig. 3 The detector

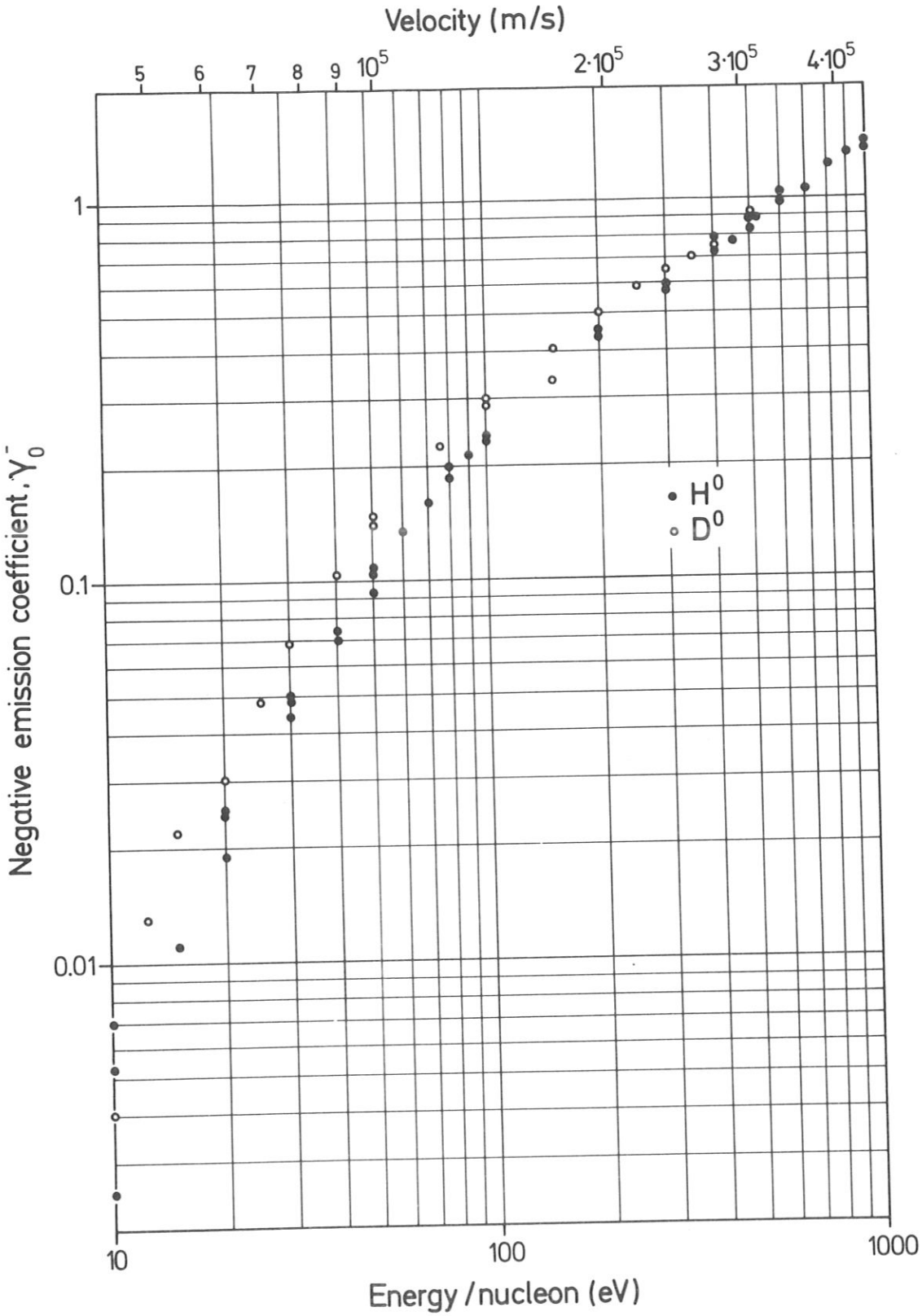

Fig. 4 Negative emission coefficient $\gamma(E)$ for H^0 and D^0 impinging on the Cu converter electrode of the detector shown in Fig. 3.

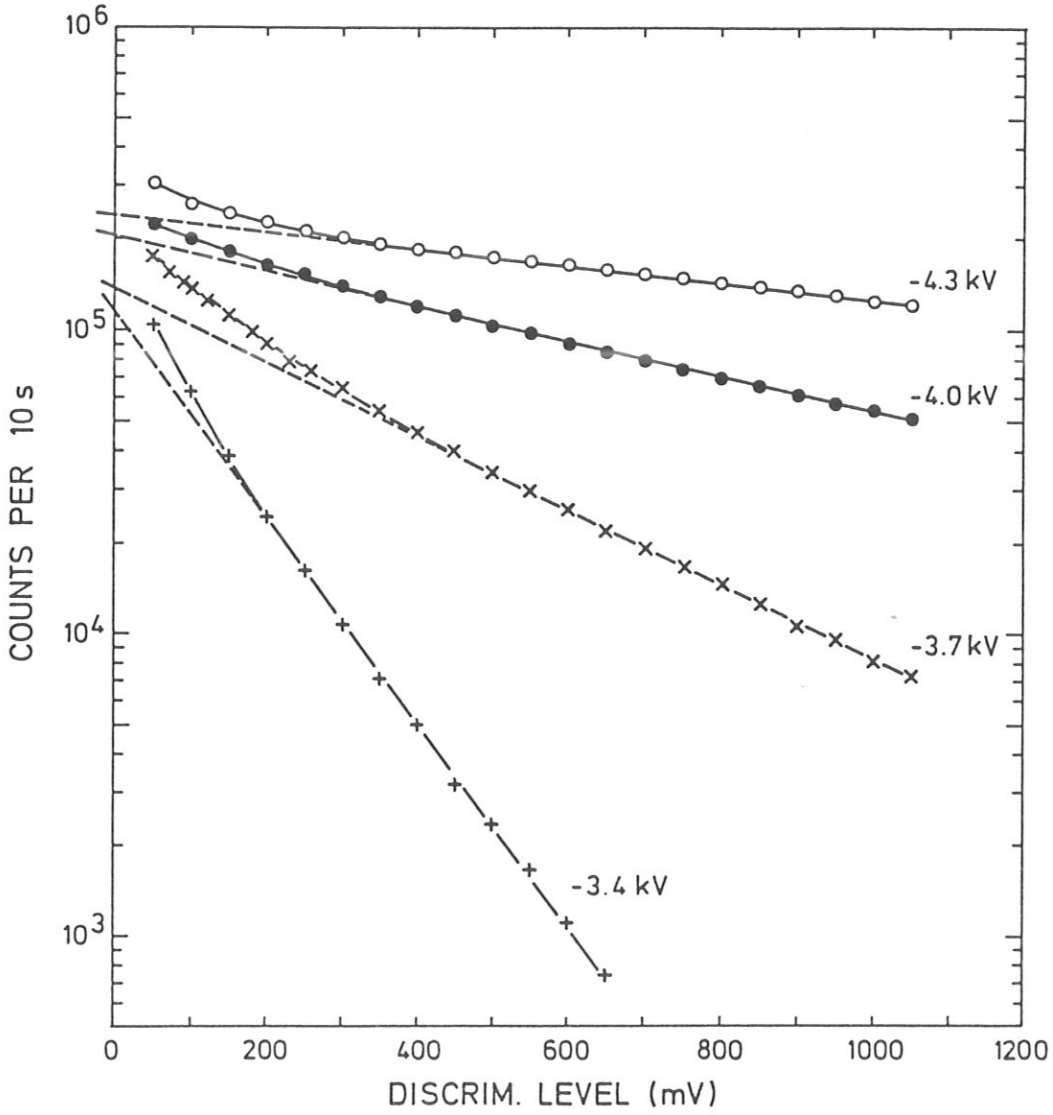

Fig. 5 Count rate versus discriminator level for different multiplier voltages during a glow discharge in ASDEX

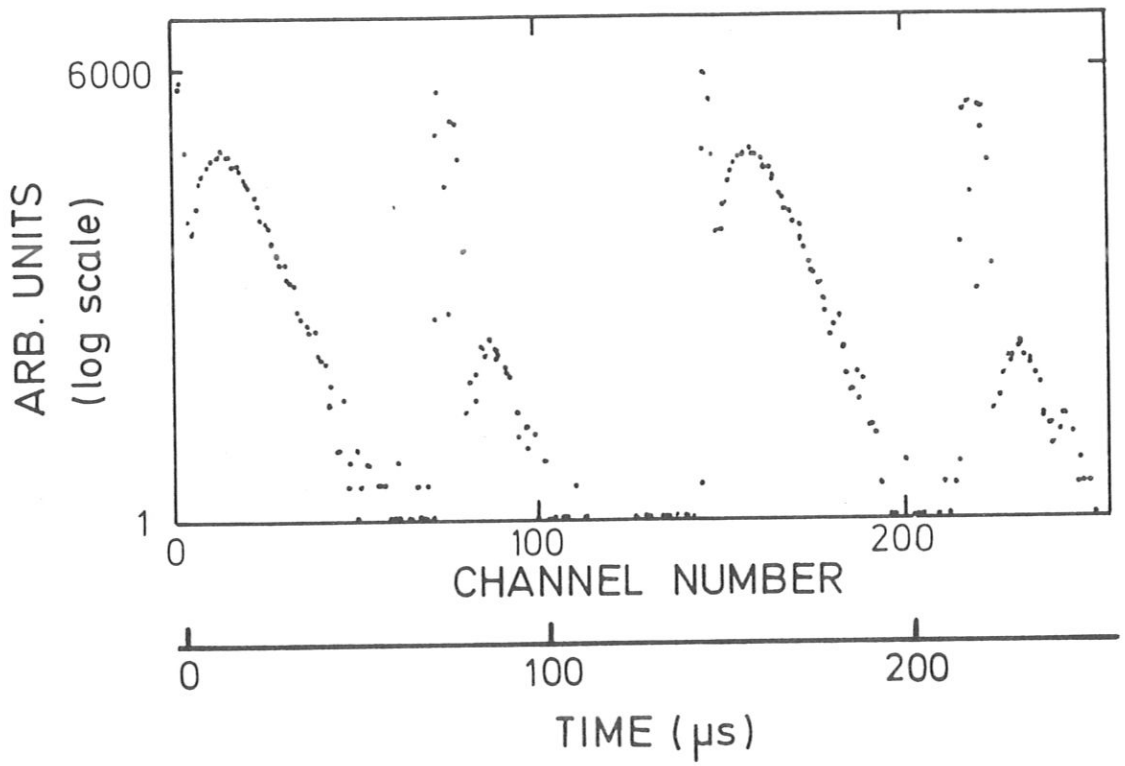

Fig. 6 Arrival time distribution as stored in the MCA

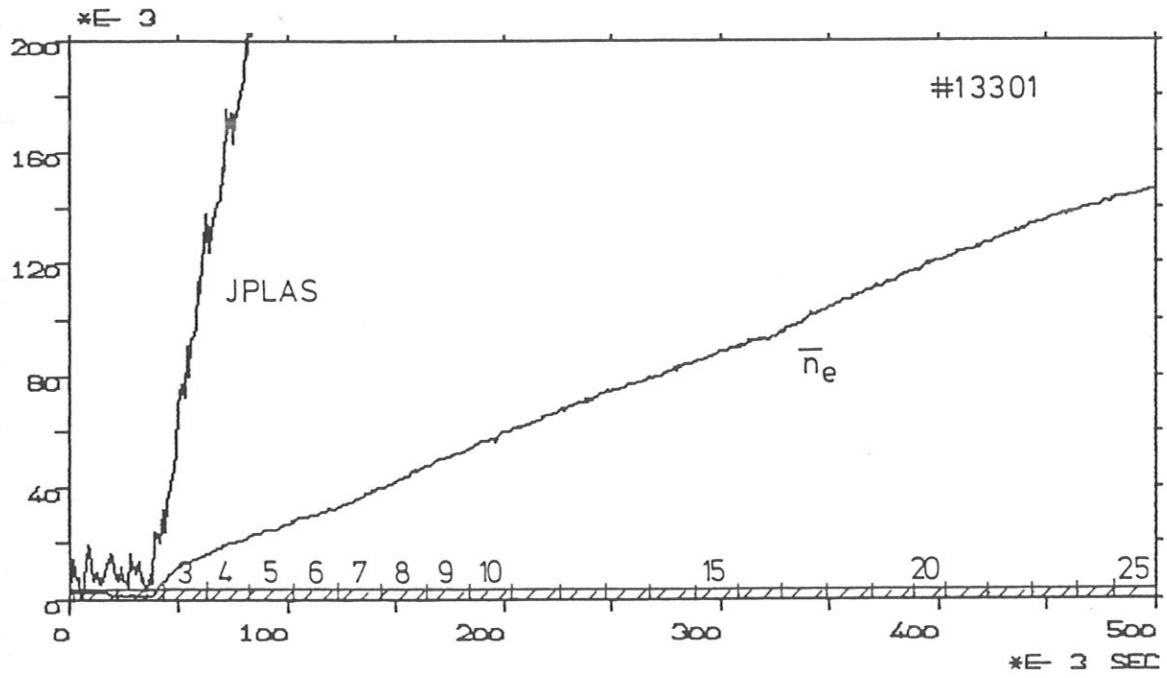

Fig. 7 Line averaged electron density and plasma current in the first 500 ms of ASDEX shot # 13301.
Vertical full scale ≙ 2.76 x 10^{13} cm^{-3}. Deuterium plasma.

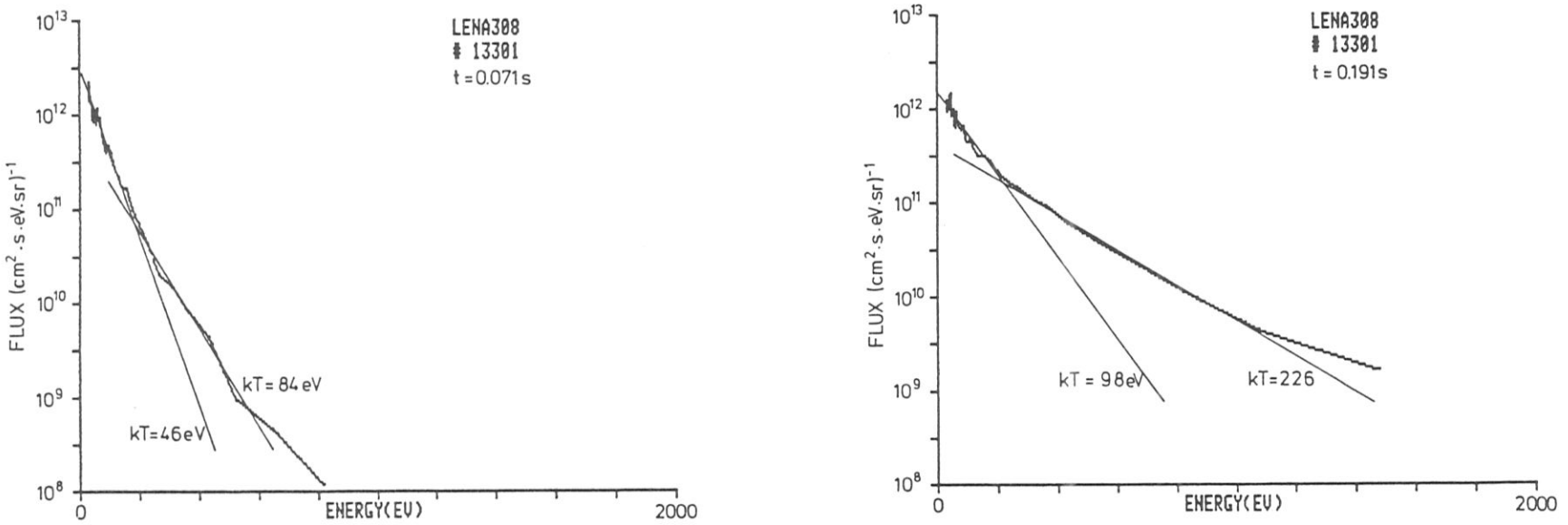

Fig. 8 Differential neutral emission spectra at 0.07 s and 0.19 s of shot # 13301 shown in Fig. 7.

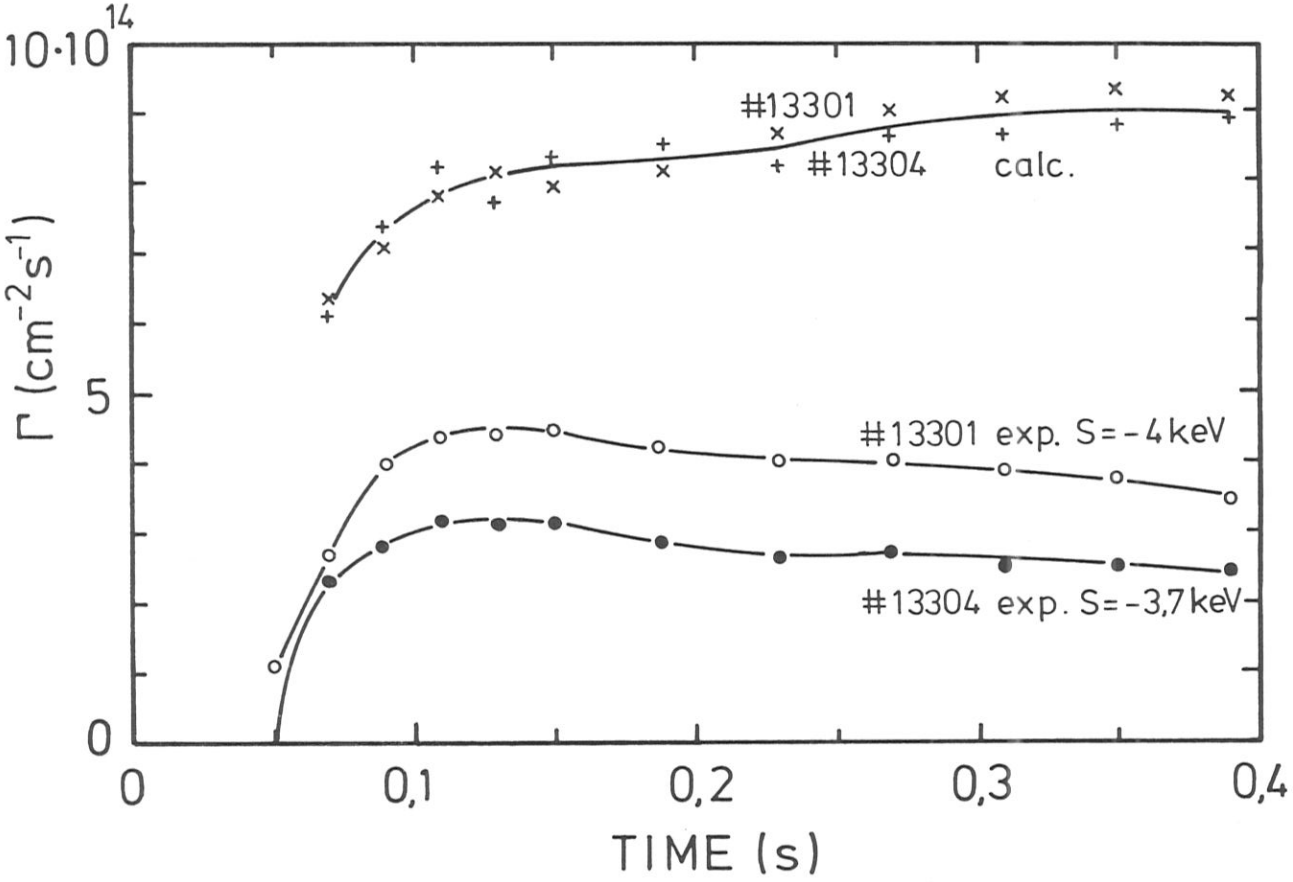

Fig. 9 Neutral emission during plasma start up. Upper curve: calculated according to equ. 6; lower curves: experimental for 2 shots with different multiplier voltages.

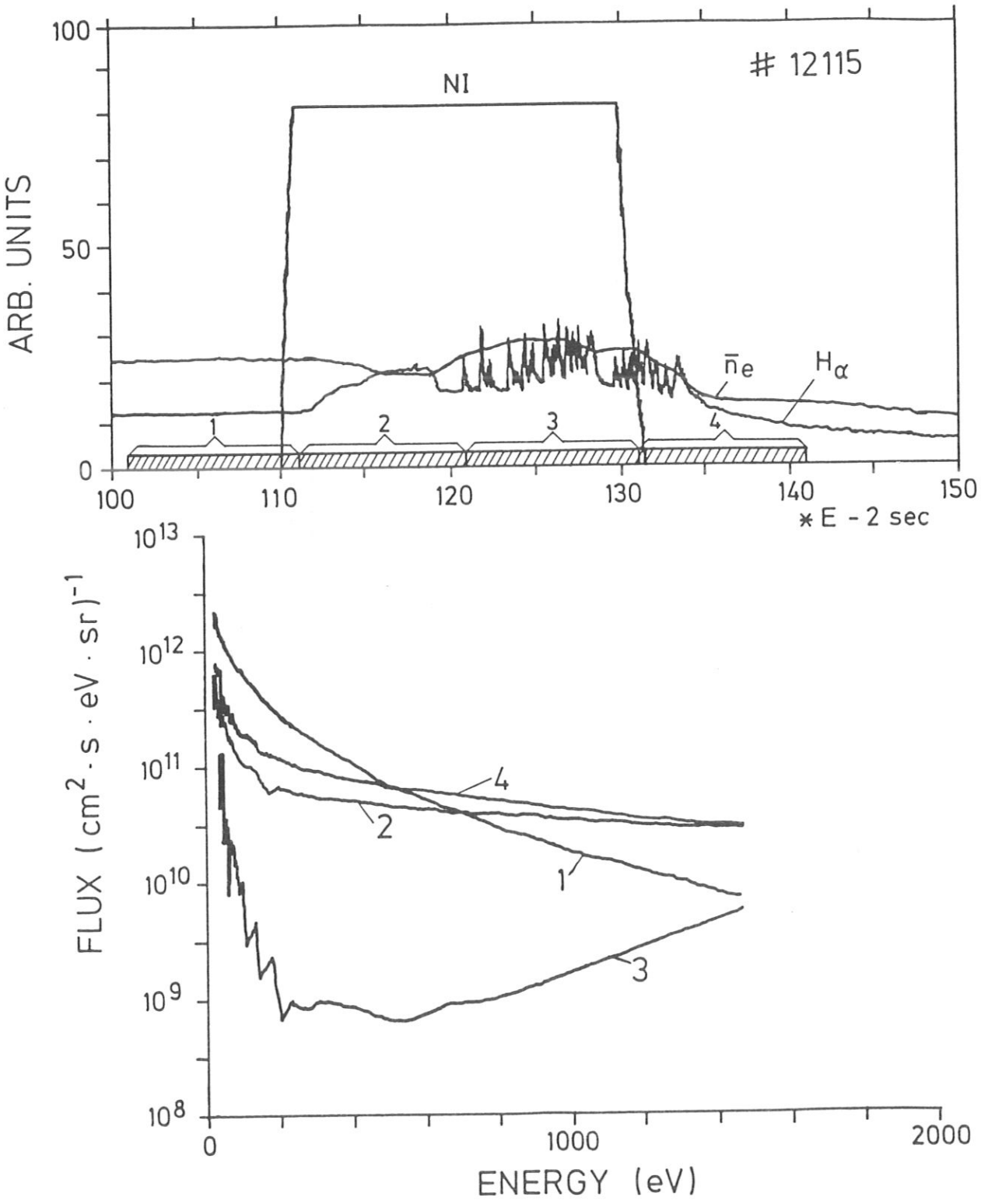

Fig. 10 $\bar{n}_e$ and H_α-emission of # 12115 during the neutral injection phase (NI). Deuterium plasma, H^0-injection by 8 sources.
Differential neutral emission spectra during the times indicated in upper fig.

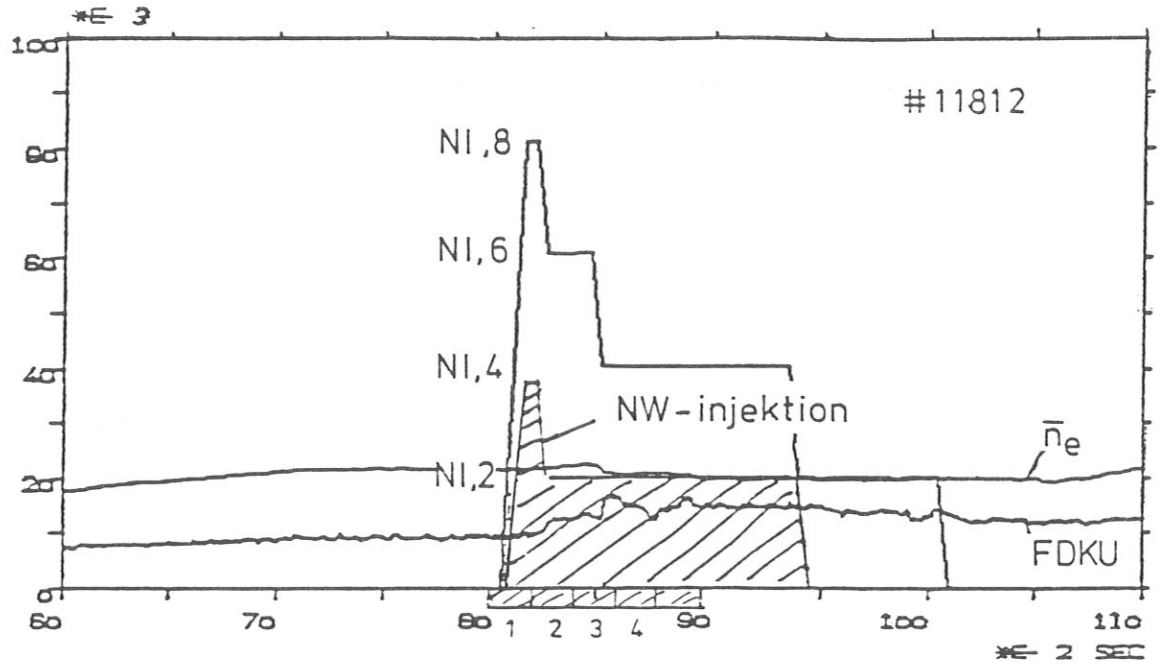

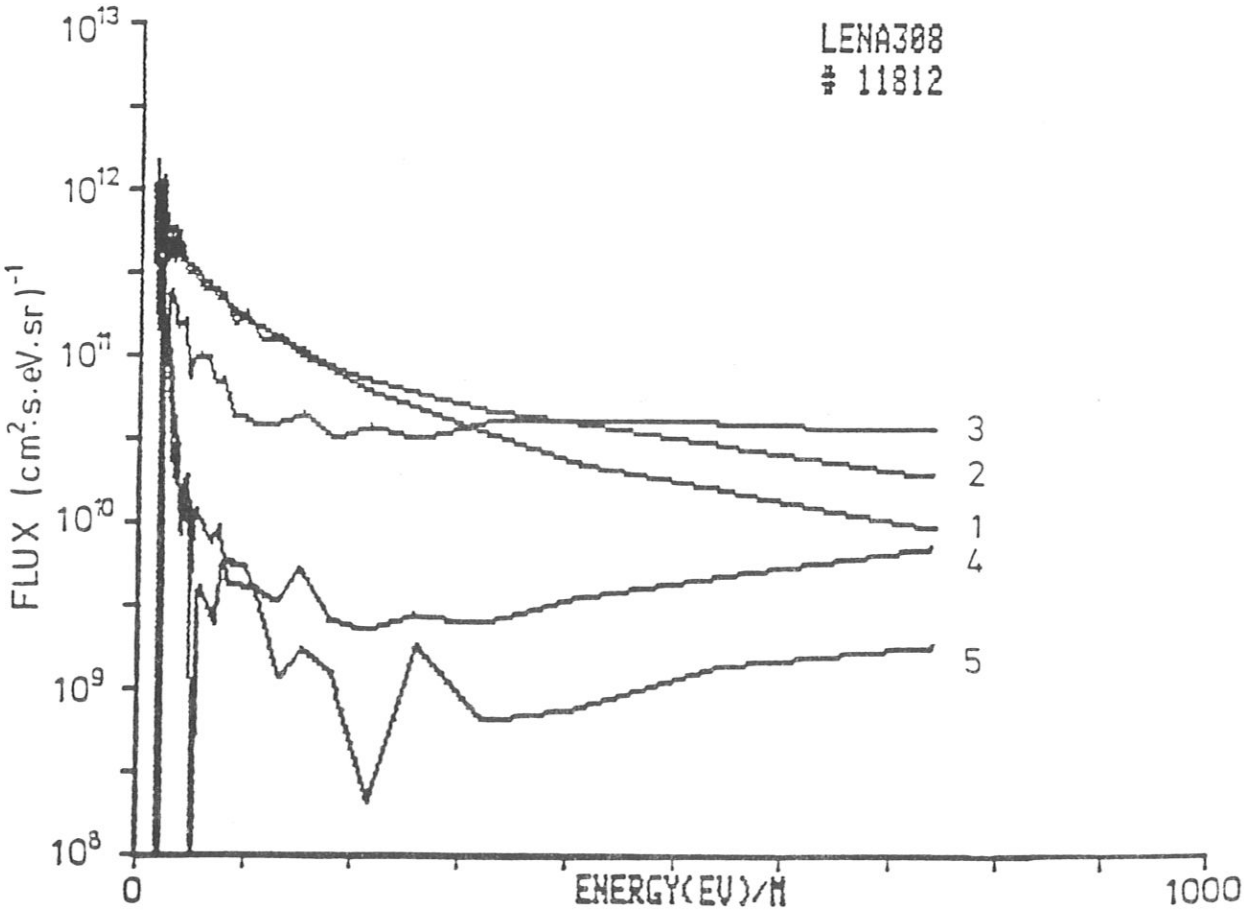

Fig. 11 $\bar{n}_e$ and H_α-emission (FDKU) of # 11812. Deuterium plasma, D^0 injection by 8, 6 and 4 sources.
Differential neutral emission spectra during the times indicated in upper fig.

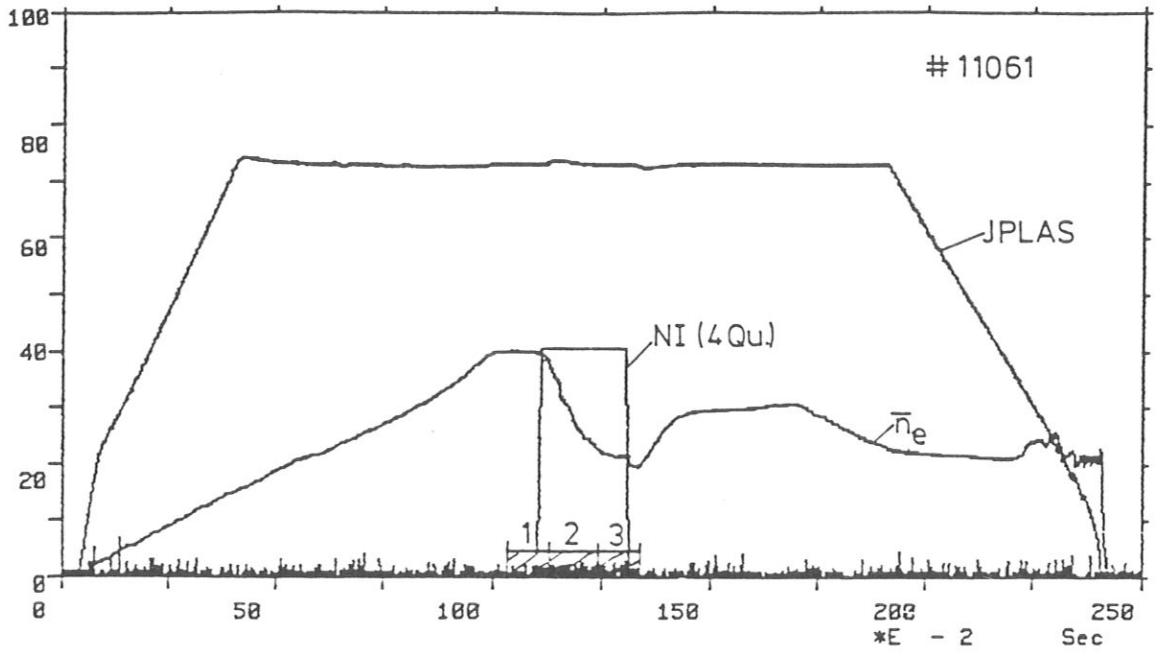

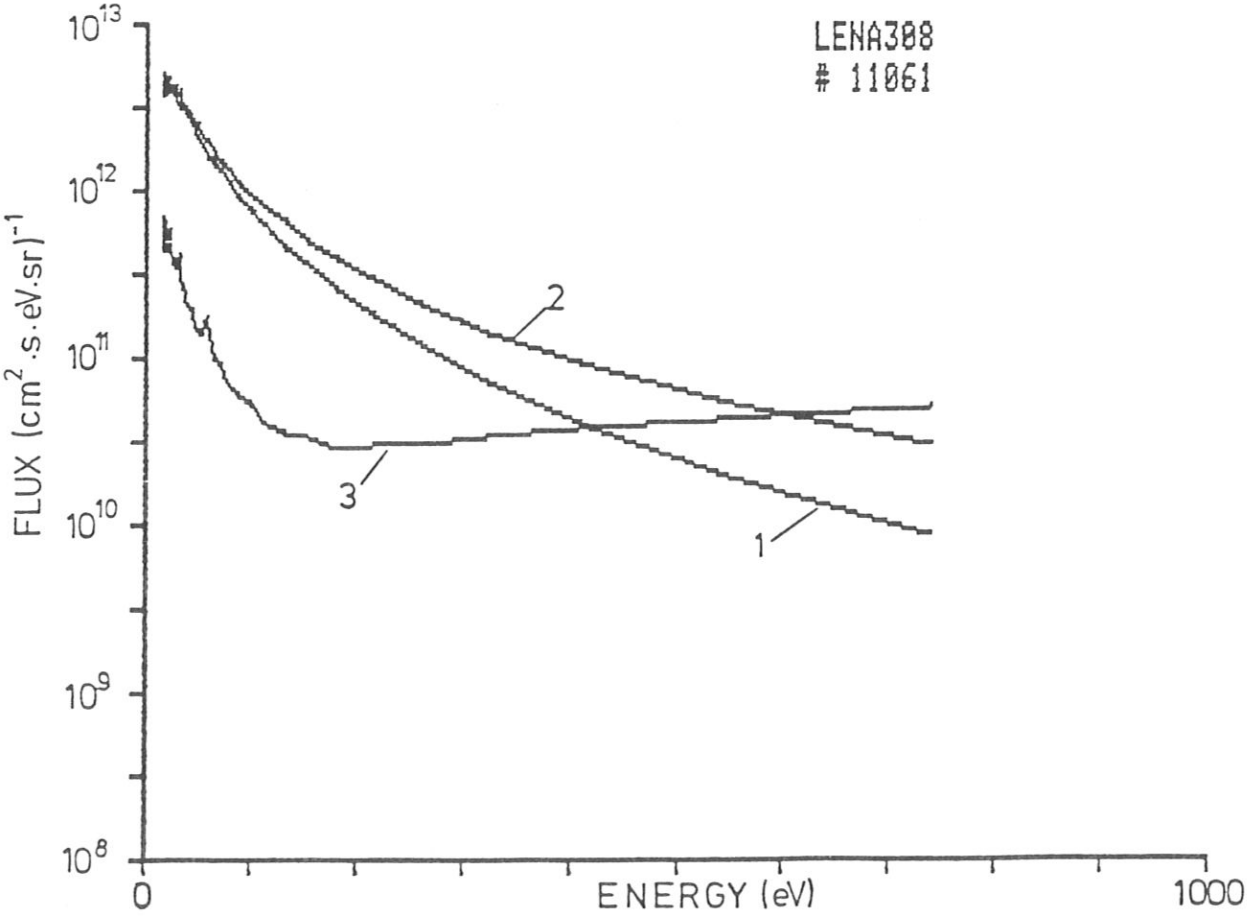

Fig. 12 $\bar{n}_e$ and plasma current of # 11061. Hydrogen plasma, H^0-injection by 4 sources.
Differential neutral emission spectra during times indicated in upper fig.

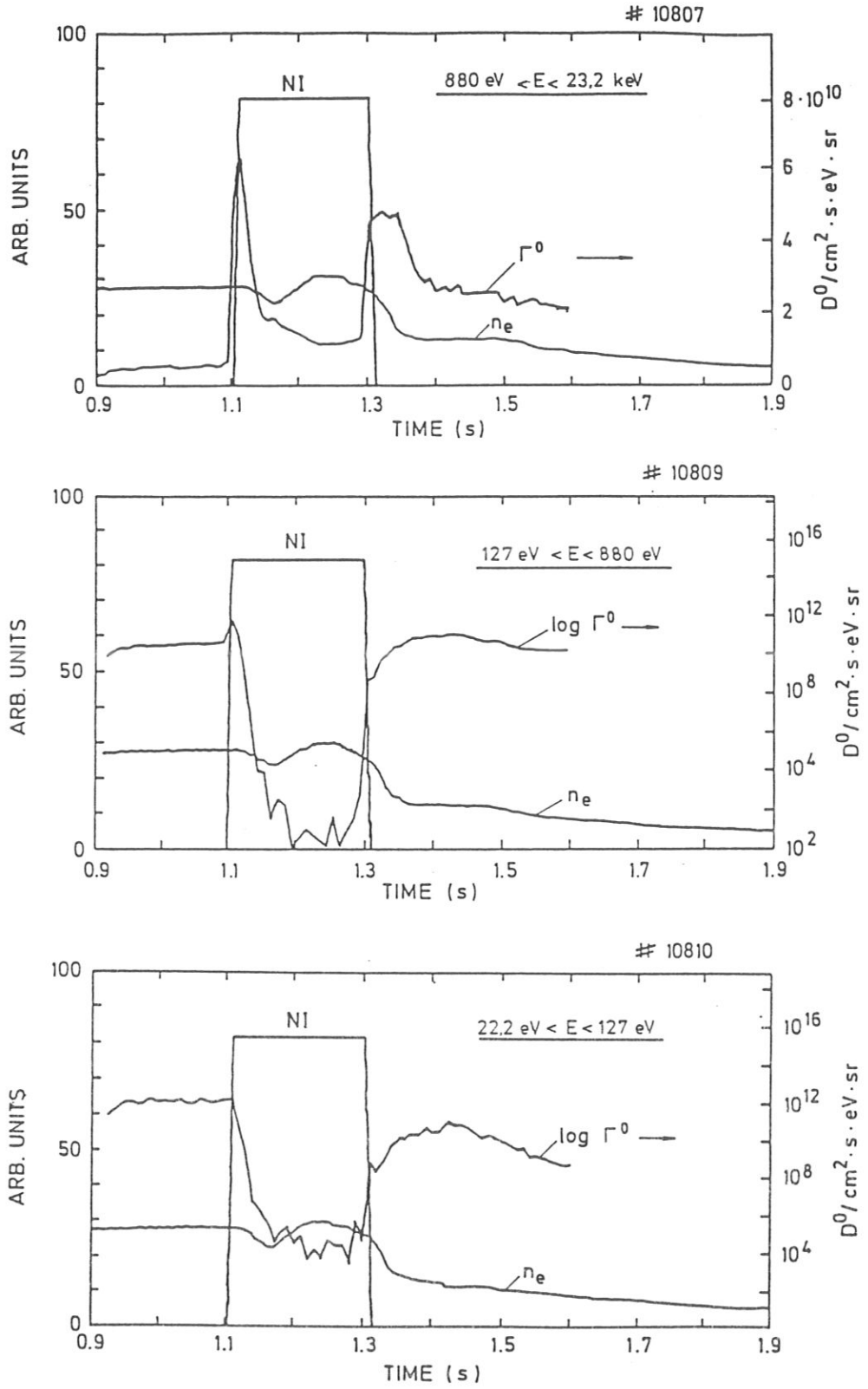

Fig. 13 Neutral emission Γ in different energy intervals during neutral injection. All shots were Deuterium discharges with H^0-injection (8 sources).

Note: Γ scale is linear for # 10807 and logarithmic for # 10809 and # 10810.

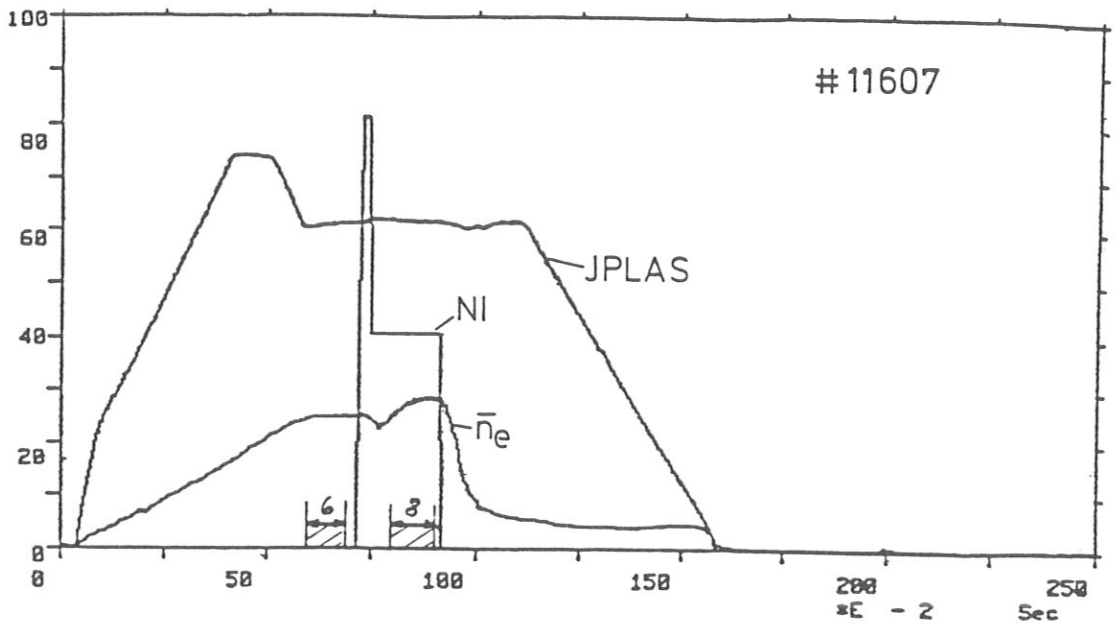

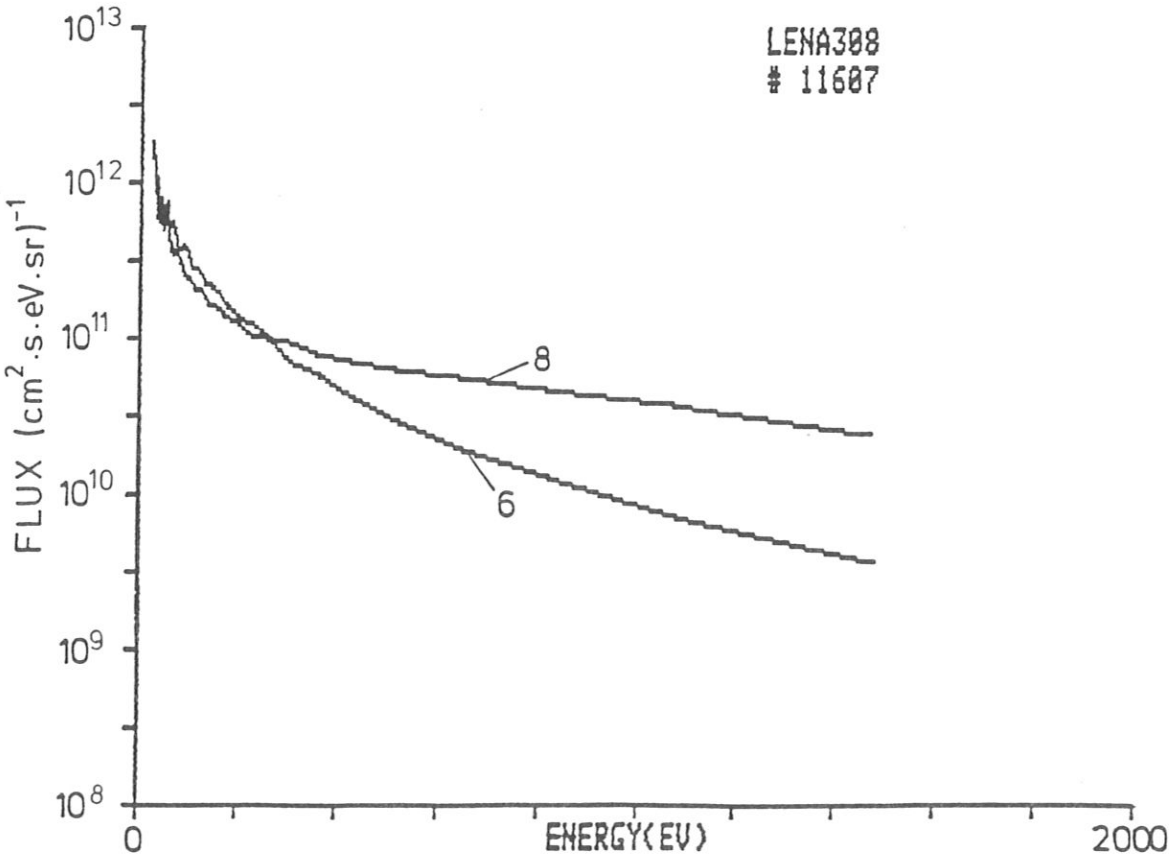

Fig. 14 $\bar{n}_e$ and plasma current for # 11607. Deuterium plasma, D^0 injection (after ignition 4 sources of 8 failed). Plasma shifted upward ($\Delta Z = 2$).

Differential neutral emission spectra at times indicated in upper fig.

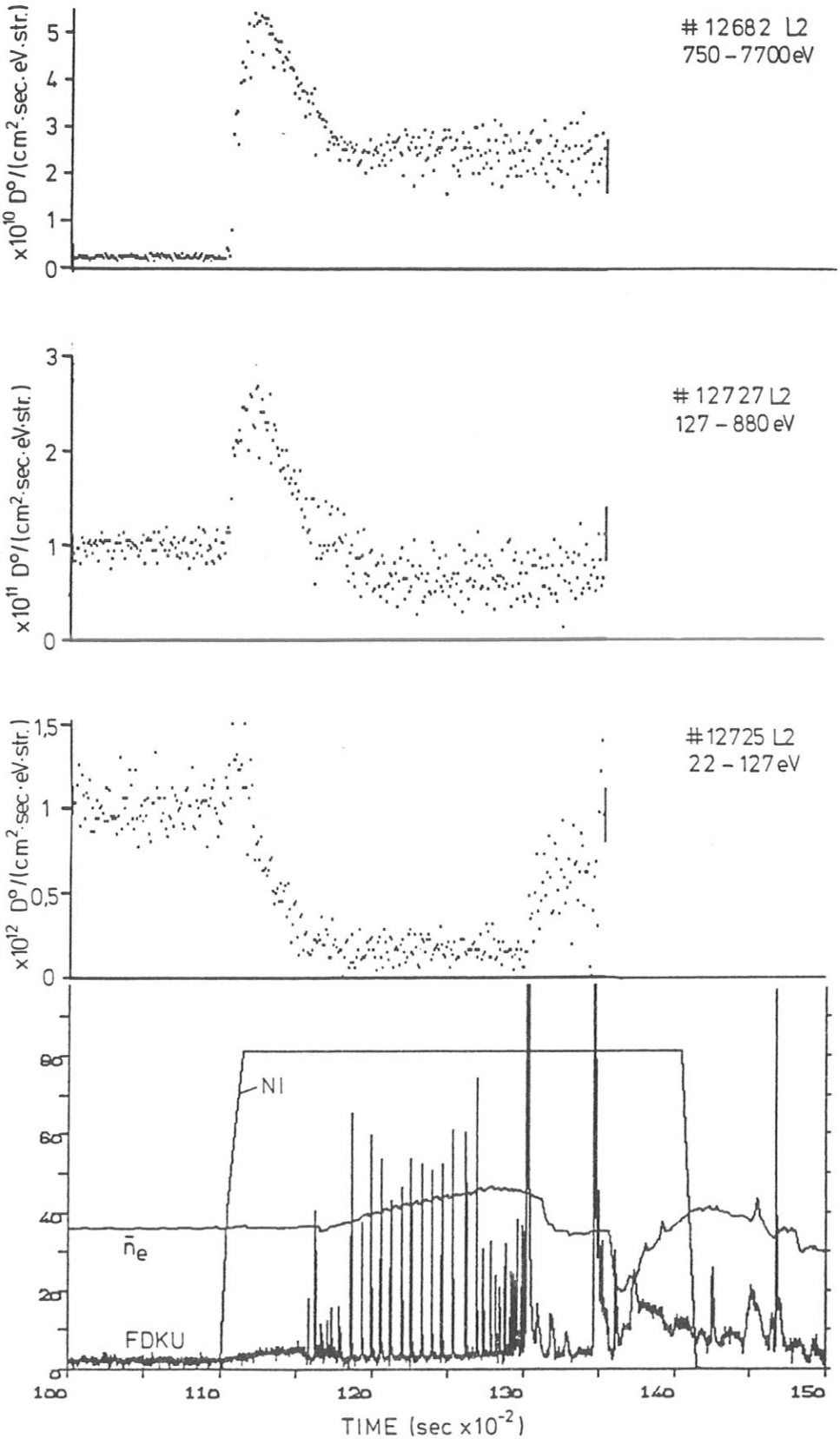

Fig. 15 Neutral emission Γ in different energy intervals during NI. All shots were Deuterium discharges with D^0-injection by 8 sources of same kind as indicated at bottom picture. Plasma shifted upward ($\Delta Z = 2$).

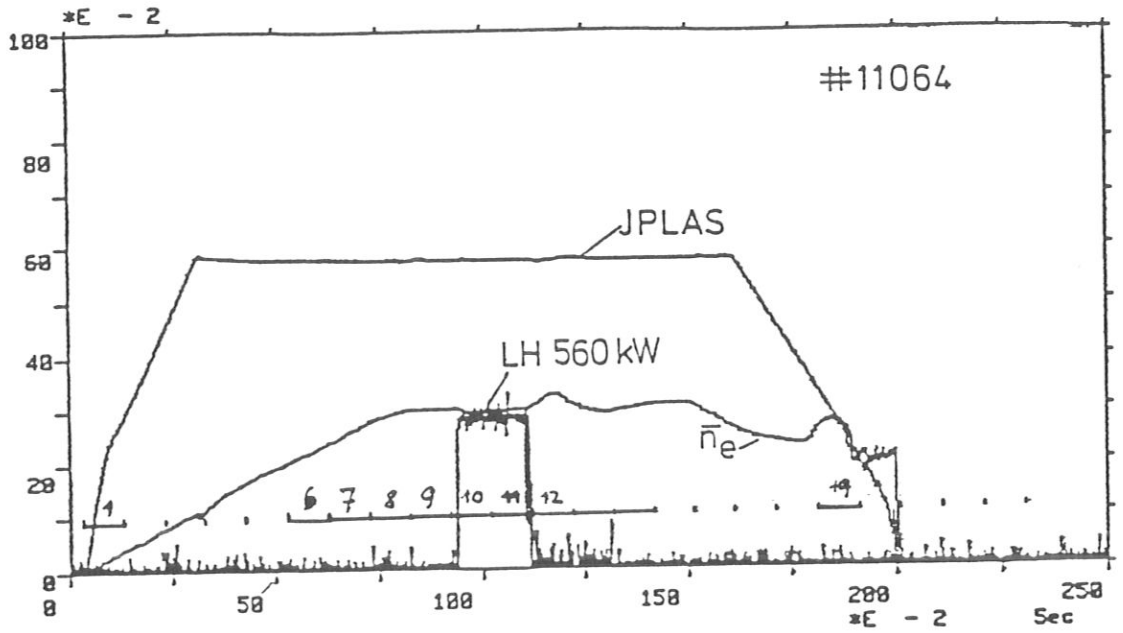

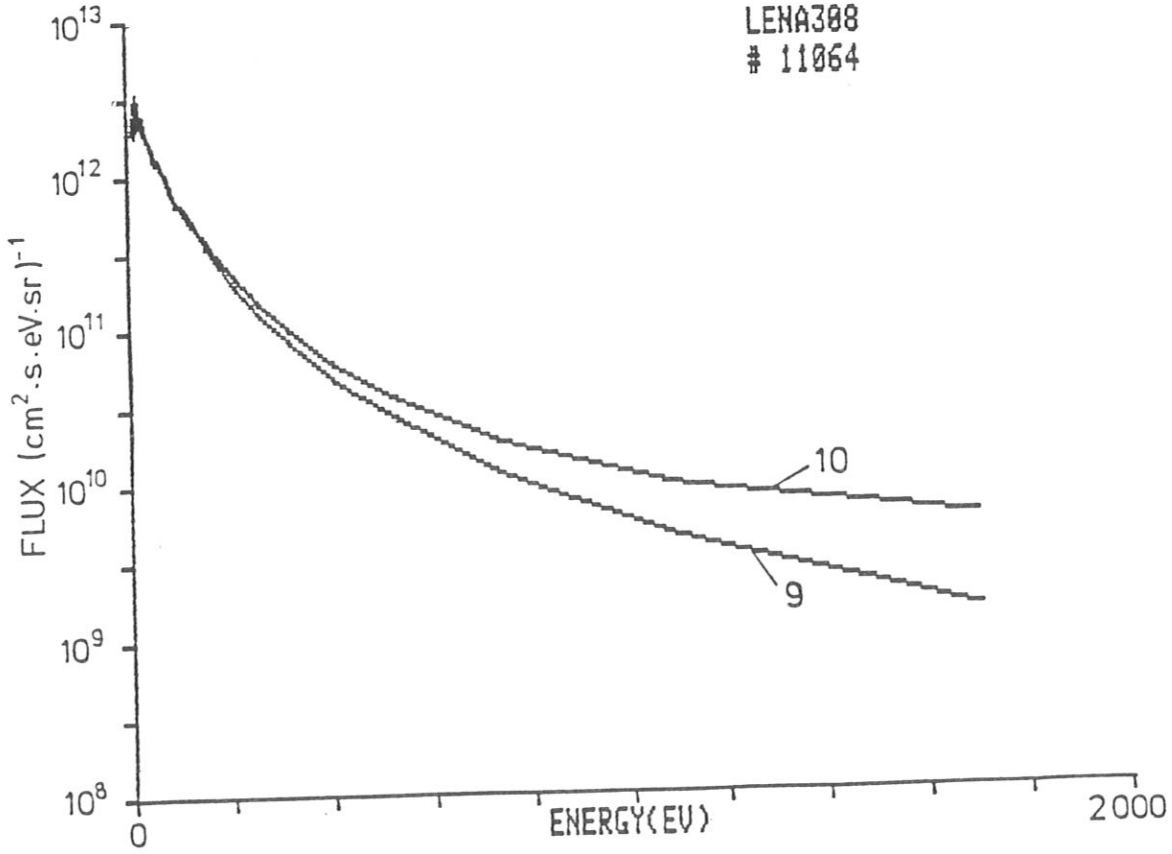

Fig. 16 $\bar{n}_e$ and plasma current of # 11064, hydrogen plasma, lower hybrid resonance heating between 0.9 and 1.1 sec. Differential neutral emission spectra before and during LH.

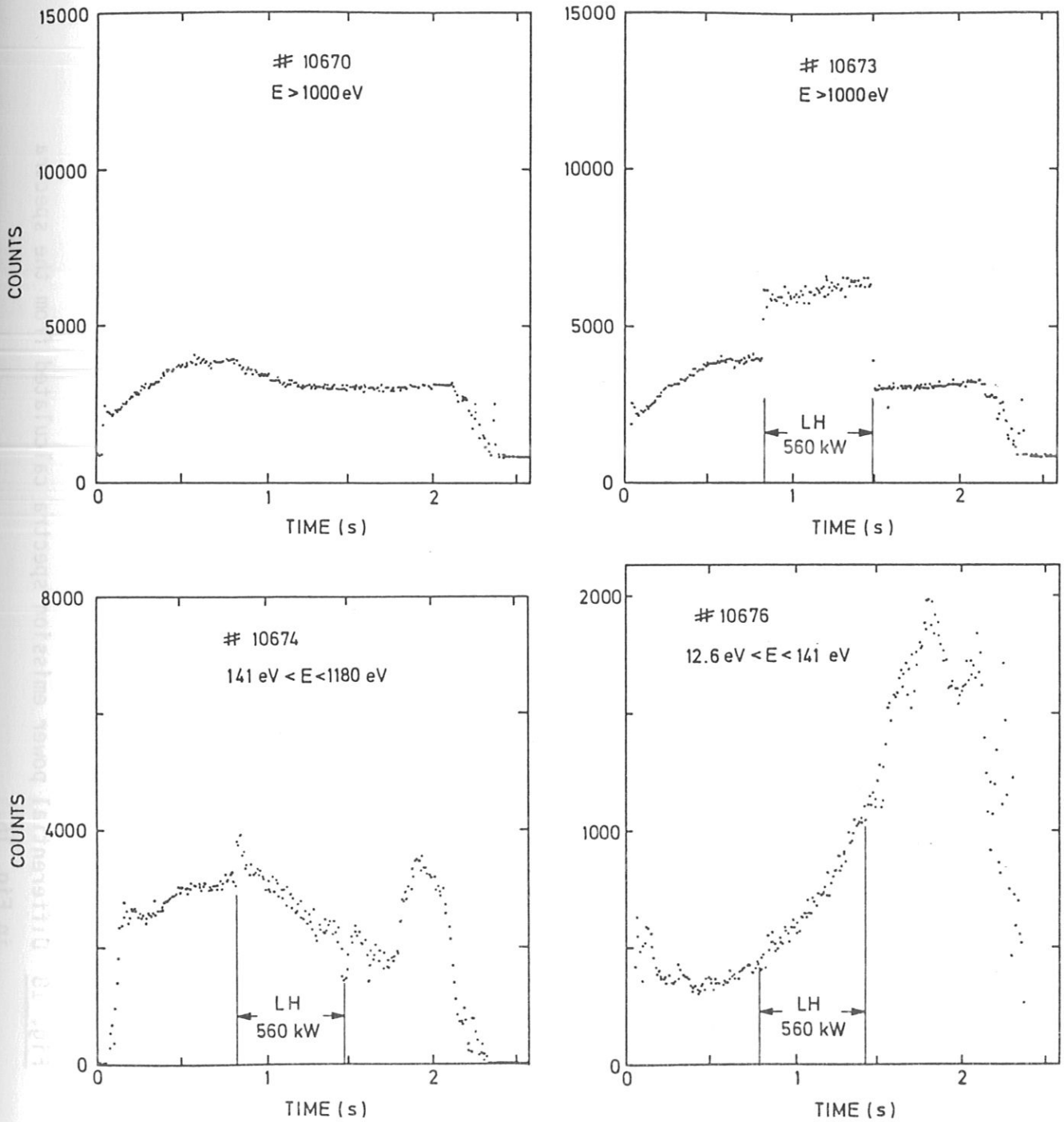

Fig. 17 Neutral emission Γ in different energy intervals during lower hybrid resonance heating. No LH for upper left fig. Hydrogen plasma.

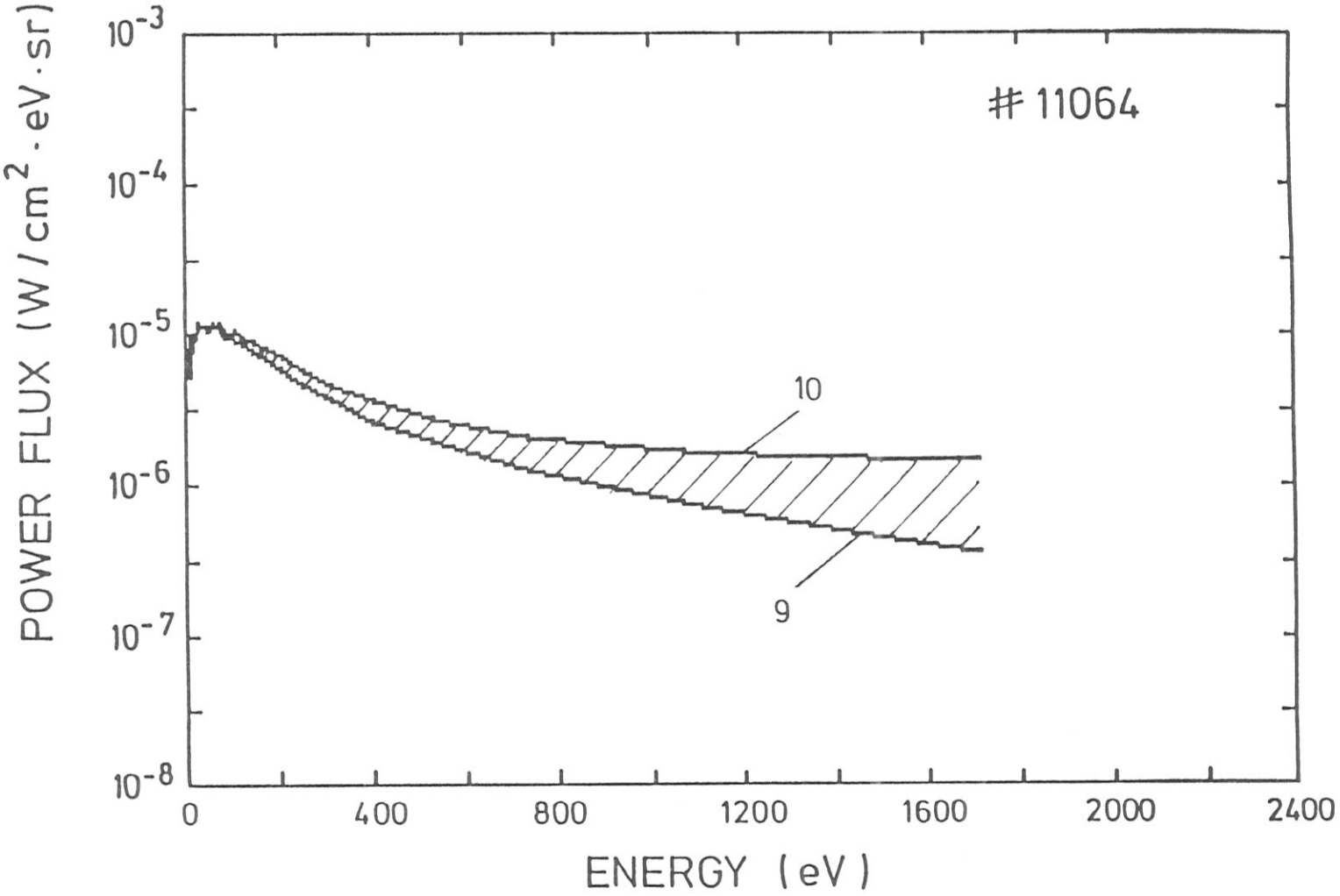

Fig. 18 Differential power emission spectra calculated from the spectra in Fig. 16.

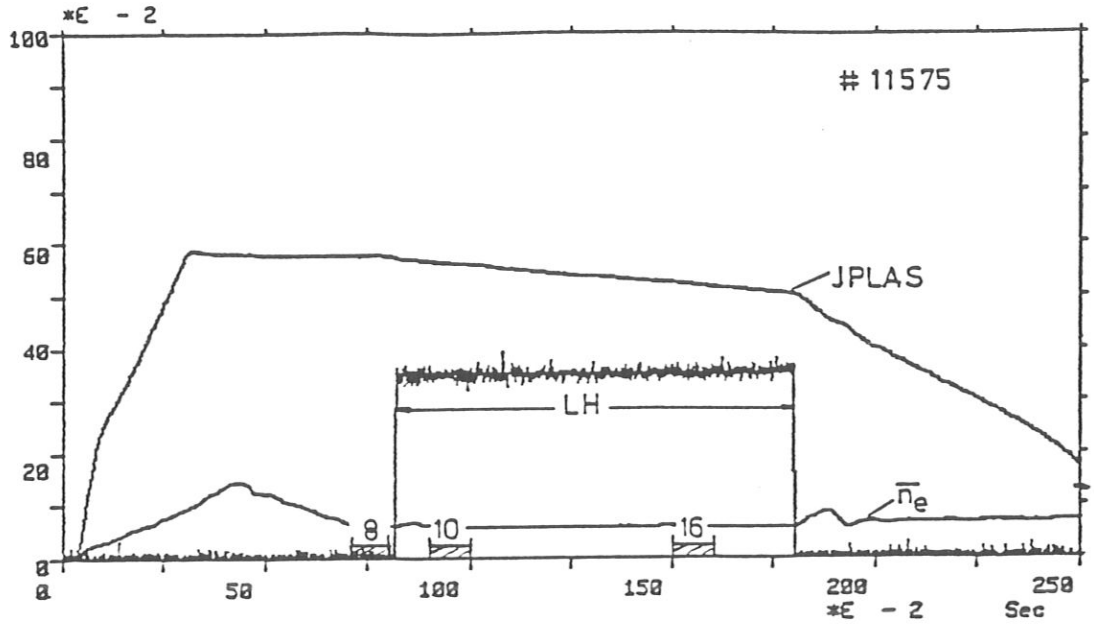

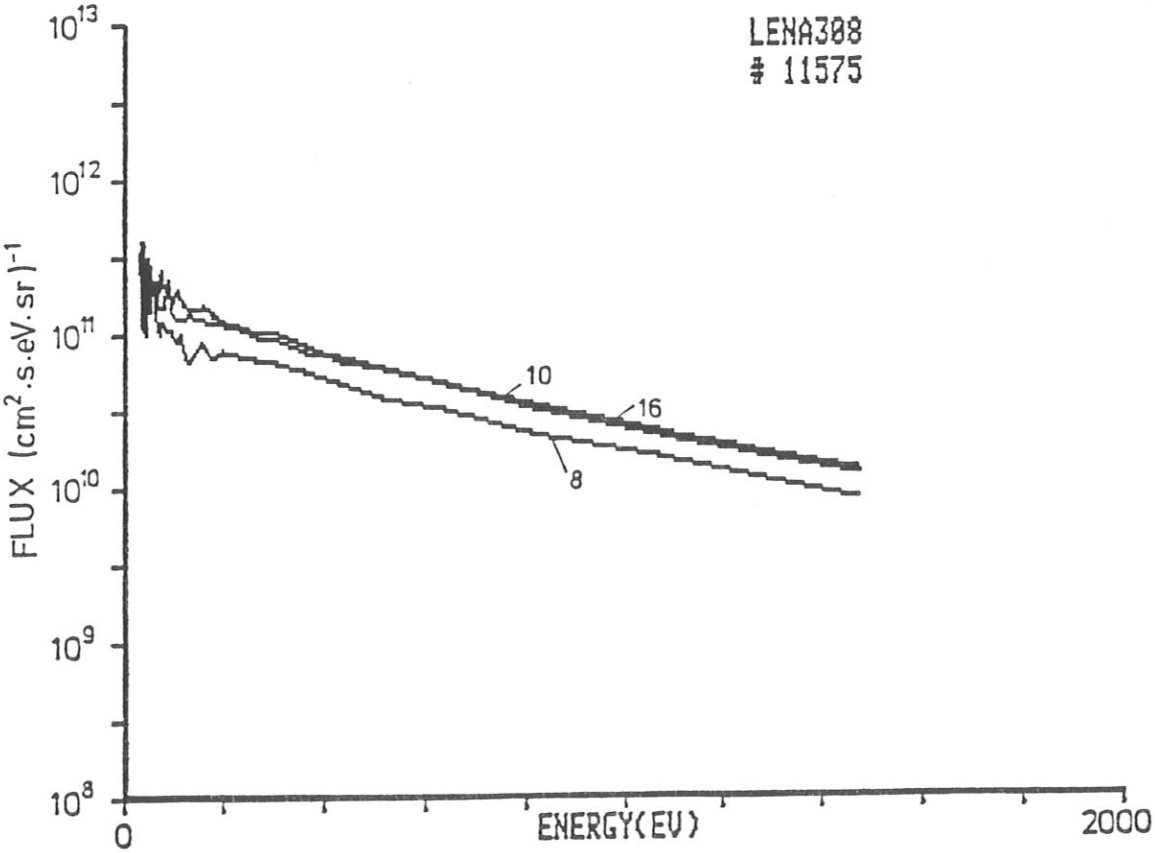

Fig. 19 $\bar{n}_e$ and plasma current of #11575, current drive by LH between 0.8 and 1.8 sec. Deuterium plasma.
Differential neutral emission spectra before and during LH.

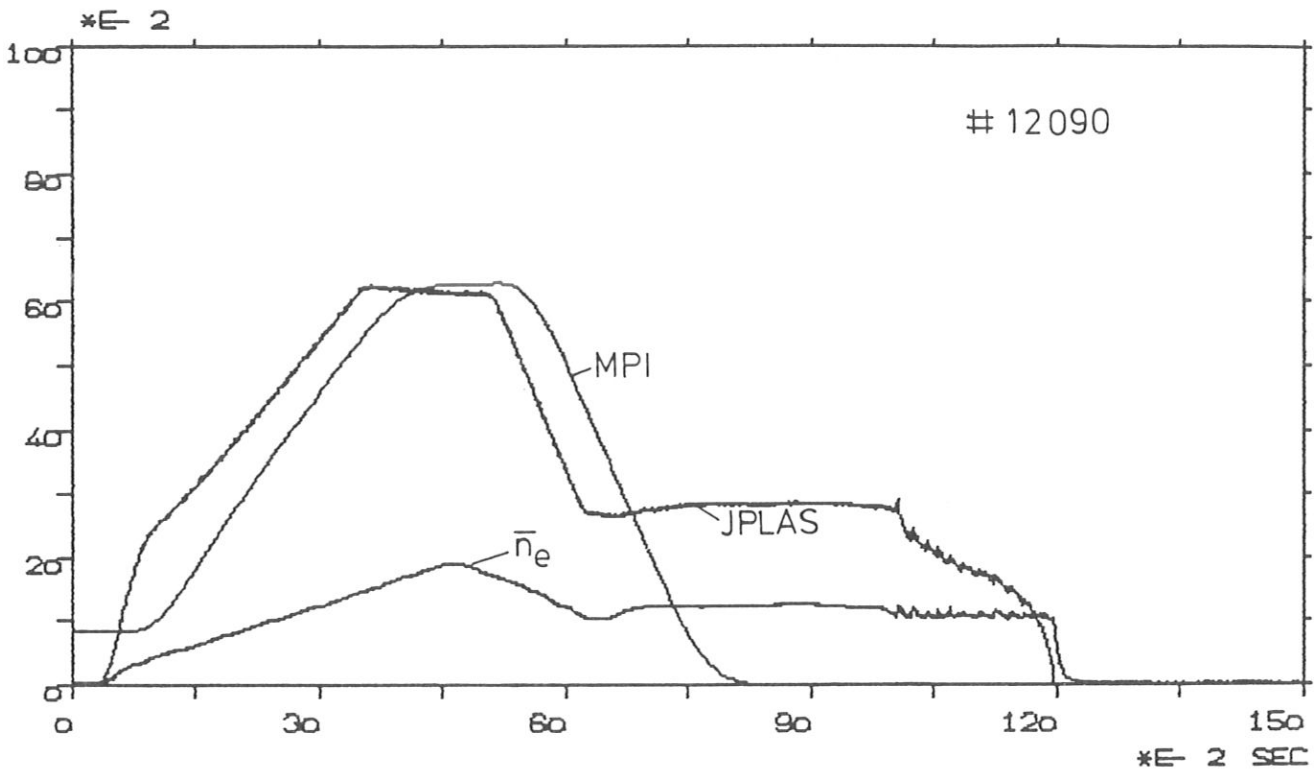

Fig. 20 $\bar{n}_e$ and plasma current of #12090. Multipole current MPI was tuned to zero for limiter operation. Deuterium plasma.

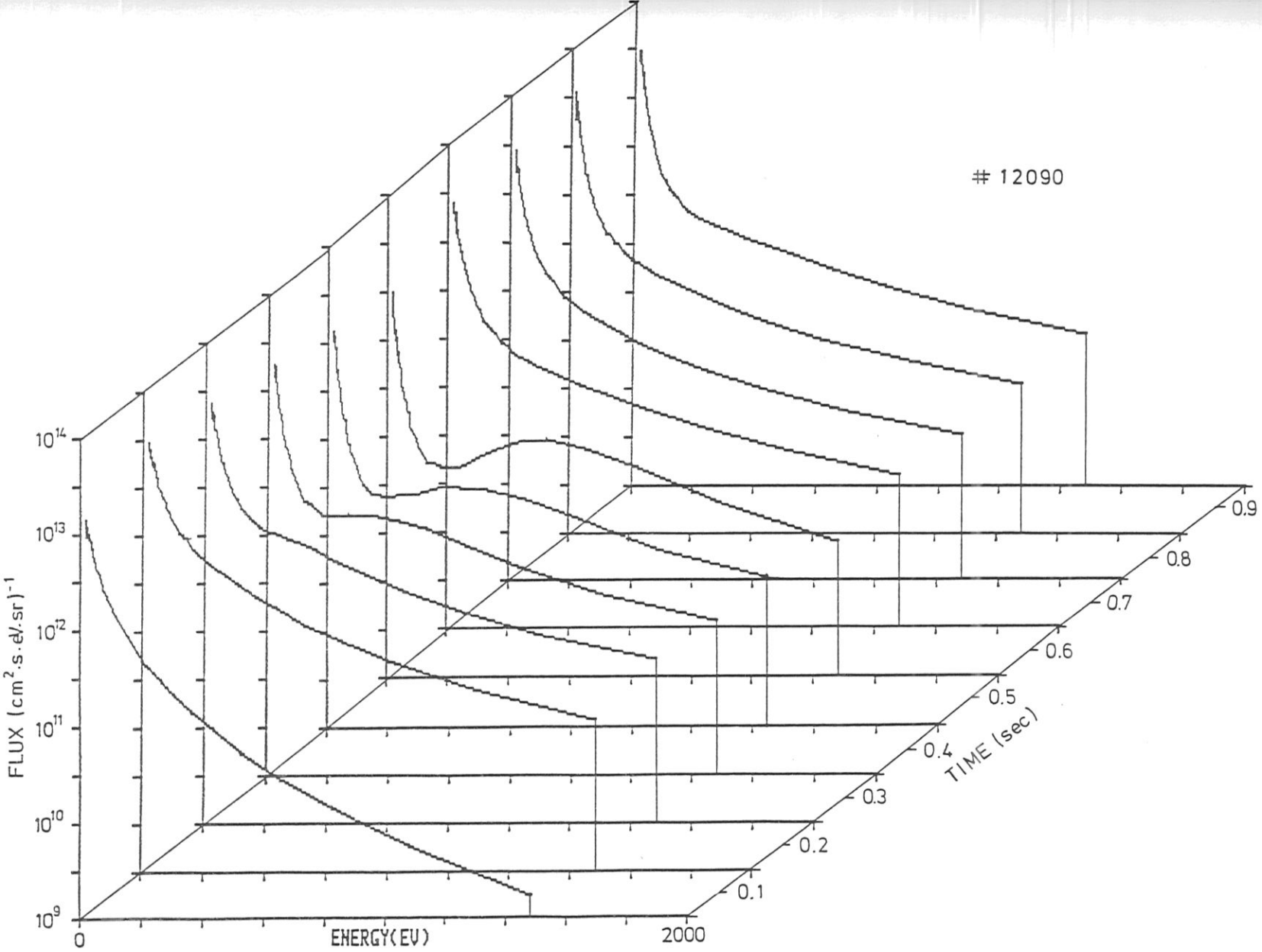

Fig. 21 Development of the differential neutral emission spectra during shot # 12 090.